

# Regularity and chaos in the nuclear masses

Patricio Leboeuf

Laboratoire de Physique Théorique et Modèles Statistiques,\*  
Bât. 100, Université de Paris-Sud, 91405 Orsay Cedex, France

**Summary.** Shell effects in atomic nuclei are a quantum mechanical manifestation of the single-particle motion of the nucleons. They are directly related to the structure and fluctuations of the single-particle spectrum. Our understanding of these fluctuations and of their connections with the regular or chaotic nature of the nucleonic motion has greatly increased in the last decades. In the first part of these lectures these advances, based on random matrix theories and semiclassical methods, are briefly reviewed. Their consequences on the thermodynamic properties of Fermi gases and, in particular, on the masses of atomic nuclei are then presented. The structure and importance of shell effects in the nuclear masses with regular and chaotic nucleonic motion are analyzed theoretically, and the results are compared to experimental data. We clearly display experimental evidence of both types of motion. [leboeuf@lptms.u-psud.fr](mailto:leboeuf@lptms.u-psud.fr)

Lectures delivered at the VIII Hispalensis International Summer School, Sevilla, Spain, June 2003 (to appear in *Lecture Notes in Physics*, Springer-Verlag, Eds. J. M. Arias and M. Lozano).

## 1 Introduction

The mass is one of the most basic properties of an atomic nucleus. In spite of its fundamental character, it is a quite complicated and highly non-trivial quantity. According to Einstein's celebrated law,  $m = E/c^2$ , all types of energy stored inside a nucleus contribute to its mass. If we imagine that the nucleons are initially separated, and then progressively move towards each other to finally form a nucleus in its ground state, a certain amount of energy  $\mathcal{B}$  will be released in the process. Mathematically, this corresponds to the equation,

$$Mc^2 = \sum_j m_j c^2 - \mathcal{B} , \quad (1)$$

where  $M$  is the mass of the nucleus,  $c$  the speed of light, and  $m_j$  the mass of the  $j$ th nucleon. The binding energy  $\mathcal{B}$  is responsible for the cohesion of the system, the larger  $\mathcal{B}$  is, the more stable is the nucleus. There are different sources to this energy. The most important one comes from the strong attractive interaction between nucleons. Other interactions and effects that contribute to  $\mathcal{B}$  are the Coulomb repulsion between protons, the surface effects, etc. In phenomenological descriptions of the mass, these contributions

\* Unité de Recherche de l'Université Paris XI associée au CNRS

are usually taken into account by, for example, liquid drop expressions à la von Weizsäcker [1]. There is another important contribution. In a semiclassical picture where each nucleon is thought of as an individual particle moving in a mean-field potential, this contribution is related to the motion of the nucleons inside the nucleus. Because of Pauli's exclusion principle, when the nucleons are put together to form a bound system they are not at rest, but instead move with a speed which is of the order of  $0.3c$ . Via Einstein's relation, this kinetic energy also contributes to  $\mathcal{B}$ , and therefore to the mass. Part of this energy, namely the one that varies smoothly with the number of nucleons, is already taken into account in the phenomenological liquid drop terms mentioned above. In contrast, the remaining part of the kinematic energy fluctuates with the number of nucleons. It moreover depends on the nature of the motion of the nucleons. For this reason, we refer to this contribution as the "dynamical" component of the mass.

From the theory of dynamical systems, there are two important, extreme, and distinct possibilities for the motion of the nucleons inside the nucleus, namely it can be either regular or chaotic. A natural question to ask concerns the relation between these two types of motion and the properties of the associated dynamical mass. Is it possible to distinguish between a "regular" and a "chaotic" mass? How can the difference be detected experimentally, if any? The purpose of these lectures is to bring some answers in this direction. We will show that it is indeed possible to make the difference between both types of dynamical masses via their fluctuation properties, i.e., how the mass varies as a parameter, typically the number of nucleons, is changed. When the results are applied to the available experimental data, the analysis of both types of dynamical masses indicates that, apart from a dominant regular component that will be described in some detail via a spheroidal potential, there might be in addition some chaos in the ground state of the nucleus. The corresponding contribution to the mass and its dependence with the number of nucleons will be explicitly computed. It will be shown that the hypothesis of chaotic layers explains the observed differences between the experimental data and previous theoretical calculations.

Although the setting we are using is based on a single-particle picture of the nucleus, several arguments indicate that the results obtained are of more general validity. They may in fact be related to correlations acting between nucleons that are beyond a mean-field picture.

Traditionally, dynamical effects in the structure of nuclei are referred to as shell effects. This designation originated in atomic physics, where the symmetries of the Hamiltonian produce strong degeneracies of the electronic levels (the shells). These degeneracies induce, in turn, oscillations in the electronic binding energy. Shell effects are therefore due to deviations (or bunching) of the single-particle levels with respect to their average properties. The degeneracies of the electronic levels of an atom produced by the rotational symmetry are an extreme manifestation of level bunching. In general, in systems that

have other symmetries, or have no symmetries at all, there will still be level bunching, but its importance will typically be minor. Therefore, depending on the presence or absence of symmetries, the shell effects may be more or less important. The level bunching, and more generally the fluctuations of the single-particle energy levels, are thus a very general phenomenon. The theories that describe those fluctuations make a neat distinction between systems with different underlying classical dynamics (e.g., regular or chaotic). It is therefore our purpose, before entering in the discussion of the nuclear masses in §5, to give a general (though elementary) presentation of the fluctuation properties of the level density (§2 and 3), and of the way these fluctuations manifest in the different thermodynamic properties of a Fermi gas (§4). It will be shown, in particular, that generically the size of the fluctuations is more important when the classical underlying motion is regular, as compared to the chaotic case. This fact may seem paradoxical, since we are usually willing to associate chaos with noise and fluctuations. However, concerning the shell effects in quantum mechanics, the situation is exactly the other way around: because of the instability of the classical orbits, level clustering is less important in chaotic systems. We will precisely quantify the difference for several thermodynamic quantities. We will moreover discuss universality, e.g. the validity in large classes of systems of common features of the fluctuations.

The “dynamical” or shell fluctuations of the mass [2, 3] considered here are a particular example of a general phenomenon. Similar fluctuations are expected to occur, with different degrees of importance, in all thermodynamic quantities of a fermionic gas. This point is discussed in some detail in §4. Many illustrative examples may be mentioned, like the fluctuations of the persistent currents in mesoscopic rings, the force fluctuations observed when pulling a metallic nanowire, or the supershell structure in metallic particles. They all have the same physical origin, which in the context of semiclassical theories is associated to classical periodic orbits. See for example Ref. [4] for a discussion in condensed matter mesoscopic physics, and Ref. [5] for cluster physics. For a general statistical theory of the fluctuations, and further related references, see Ref. [6].

These lectures are based on research carried out over the past few years, during which I have enjoyed and benefitted from collaborations with A. Monastra and O. Bohigas. I am deeply indebted to them. §4 is based on Leboeuf and Monastra, Ref. [6], and §5 on Bohigas and Leboeuf, Ref. [7]. The analysis of the regular component of the mass and of supershell structures in nuclei presented in §5, based on a spheroidal cavity with a finite lifetime for quasiparticles, is original and was not published elsewhere. References [8] and [9] report some closely related results that are not discussed here; they treat thermodynamic aspects of a fictitious element, “The Riemannium”, a schematic many body system inspired from number theory.

## 2 Local Fluctuations: Random Sequences

Consider a bound single-particle Hamiltonian  $H$ , whose quantum mechanical spectrum is given by a discrete sequence of energy levels  $\{E_1, E_2, \dots, E_i, \dots\}$ .  $H$  may either represent a self-consistent mean field approximation of an interacting system, or simply the Hamiltonian of a given one-body problem. At a given energy  $E$ , we denote the typical distance between neighboring eigenvalues, the mean level spacing, by  $\delta$ . The aim in this section is to present a short overview of some of the results that have been obtained concerning the fluctuations of the single-particle energy levels on scales of order  $\delta$ , and to establish connections with the underlying classical dynamics. Fluctuations on a scale  $\delta$  are termed “local”, compared to fluctuations on larger scales to be discussed in §3.

One of the most pervasive theories in the description of the statistical properties of sequences of numbers is the random matrix theory (RMT). Its range of applicability largely exceeds the spectra of single-particle systems, and even the frontiers of physics. For example, one can find it in the description of nuclear, atomic and molecular systems, the motion of electrons in a disordered potential, the behavior of classically chaotic systems, the study of integrable models, the description of the statistical properties of the critical zeros of the Riemann zeta function, and in problems of combinatorics. Some interesting articles and lectures covering these topics can be found in Refs. [10]–[14].

Motivated by its mathematical simplicity, one of the original ensembles introduced is the so-called Gaussian ensemble of random matrices [15], defined as the set of hermitian matrices  $H$  whose elements are Gaussian independent variables. The probability density of a given  $N \times N$  hermitian matrix is defined as

$$P(H) = c_H \exp\left(-\frac{\beta}{2} \text{tr} H^2\right), \quad (2)$$

where  $c_H$  is a normalization constant. A very specific aspect of this ensemble is its invariance under rotations in Hilbert space. The form of  $H$  depends on symmetry considerations: its matrix elements are real for even spin systems with time reversal symmetry, complex in the absence of time reversal symmetry, and quaternion for odd spins with time reversal symmetry. For these three cases, the parameter  $\beta$  in Eq. (2) takes the value 1, 2 and 4, respectively.

Given the probability density of matrix elements (2), the problem is to find the probability distribution of the associated eigenvalues  $E_i$ ,  $i = 1, \dots, N$  and eigenvectors  $\{p_k\}$  of  $H$  (the number of parameters in the parametrization  $p_k$  of the eigenvectors depends on the symmetry of  $H$ ). In the basis where  $H$  is diagonal,  $\text{tr} H^2 = \sum_i E_i^2$ . Moreover, the Jacobian of the transformation from matrix elements to eigenvalues and eigenvectors is given by [16]

$$\mathcal{J} = \frac{\partial(H_{ij})}{\partial(E_\alpha, p_k)} = \prod_{i < j=1}^N |E_i - E_j|^\beta . \quad (3)$$

The eigenvector's components are absent in this expression because of the rotational invariance of the ensembles. From these results, it follows that the joint probability density of the eigenvalues is (in an abuse of notation, we use the same symbol  $P$  as for the matrix probability density),

$$P(E_1, \dots, E_N) = c_E \prod_{i < j=1}^N |E_i - E_j|^\beta \exp\left(-\frac{\beta}{2} \sum_{i=1}^N E_i^2\right) , \quad (4)$$

where  $c_E$  is a normalization constant.

The most characteristic feature of this probability density is the existence of a strong repulsion between eigenvalues. The repulsion may be seen, in Eq. (4), from the fact that  $P \rightarrow 0$  when  $E_j \rightarrow E_i$ . Being related to the Jacobian, this repulsion is not a particular feature of the ensemble (2), but rather constitutes a very basic and general fact of most quantum mechanical systems.

From Eq. (4) the  $k$ -point correlation function,

$$R_k(E_1, \dots, E_k) = N!/(N-k)! \int \dots \int dE_{k+1} \dots dE_N P(E_1, \dots, E_N) ,$$

may be explicitly computed. We are particularly interested in the case  $k = 2$ , that defines the density of pairs of eigenvalues separated by a distance  $y = E_2 - E_1$  (when the distance  $y$  is local (i.e., on a scale  $\delta$ ), the two-point function is stationary and depends only on the difference; moreover, we are here interested in the ‘‘bulk’’ results, i.e. statistics of eigenvalues located near the center of the spectrum, far from the edges). A convenient way to characterize the function  $R_2(y)$  is through its Fourier transform,

$$K(\tau) = 2h \int_0^\infty \cos(y\tau/\hbar) [R_2(y) - \bar{\rho}^2 + \bar{\rho} \delta(y)] dy , \quad (5)$$

usually called the form factor.  $K(\tau)$  has units of time;  $\bar{\rho}$  is the average density of states,

$$\bar{\rho} = \delta^{-1} = \tau_H/h , \quad (6)$$

where we have introduced the Heisenberg time, the conjugate time to the mean level spacing  $\delta$ . From Eq. (4), the random matrix form factor is found to be [16],

$$K_{rmt}(\tau) = \begin{cases} \left[ 2\tau - \tau \log\left(1 + \frac{2\tau}{\tau_H}\right) \right] \Theta(\tau_H - \tau) + \\ \left[ 2\tau_H - \tau \log\left(\frac{2\tau + \tau_H}{2\tau - \tau_H}\right) \right] \Theta(\tau - \tau_H) & \beta = 1 \\ \tau \Theta(\tau_H - \tau) + \tau_H \Theta(\tau - \tau_H) & \beta = 2 . \end{cases} \quad (7)$$

For simplicity, we have restricted to  $\beta = 1$  and  $2$  (since the spin dynamics will not be included in the following, we do not consider the symplectic symmetry). In (7) the function  $\Theta$  is Heaviside's step function.  $\tau_H$  is the only characteristic time scale in Eq. (7). For short times  $\tau \ll \tau_H$ , the form factor behaves as,

$$K_{rmt}(\tau) = \frac{2}{\beta} \tau, \quad \tau \ll \tau_H, \quad (8)$$

whereas for  $\tau \gg \tau_H$  it tends to  $\tau_H$  (this is a general property of any discrete sequence of levels).

Another useful quantity is the nearest-neighbor spacing distribution  $p(s)$ , defined as the probability to find two neighboring eigenvalues separated by a distance  $s$ , where  $s$  is here measured in units of the mean level spacing  $\delta$ . Though the limiting behavior  $N \rightarrow \infty$  of  $p(s)$  may be computed analytically, the result is not explicit and it is customary to use the expression obtained from  $2 \times 2$  matrices (which turns out to differ, by accident, by only a few percent from the exact expression),

$$p(s) = \begin{cases} \frac{\pi}{2} s \exp\left(-\frac{\pi}{4} s^2\right) & \beta = 1 \\ \frac{32}{\pi^2} s^2 \exp\left(-\frac{4}{\pi} s^2\right) & \beta = 2. \end{cases} \quad (9)$$

The results obtained from RMT are usually compared to an individual system, whose spectrum has been computed numerically or measured experimentally. The statistical properties of the system are calculated in some window of size  $\Delta E$  located around an energy  $E$ . To obtain statistically significant results, an average is done by changing the position of the window. The window size  $\Delta E$  should be sufficiently large in order to include many single-particle levels and make a statistical analysis meaningful, but also it should not be too large, to guarantee that the gross features of the spectrum (e.g., the mean level spacing) are constant.

The RMT, as formulated above, is a one parameter theory. The results (see Eq. (7)) depend only on the mean level spacing  $\delta$  (or Heisenberg time  $\tau_H$ ). In order to compare different spectra coming from different physical systems, the mean spacing should be normalized. Doing this, good agreement with RMT of the local fluctuations has been found in many different situations. This is the case for example of the neutron resonances in heavy nuclei, which was the original experimental motivation to develop the RMT. Much simpler though non-trivial problems were subsequently analyzed. At the beginning of the eighties it was shown that, in the metallic regime, the statistical properties of the eigenvalues of the famous Anderson problem (e.g., an electron moving in a metal with impurities, modeled by a random 3D potential) coincide with RMT [17]. Up to now, this is the only case where the agreement with RMT was proved rigorously, though the model is not fully deterministic (randomness is incorporated by hand in the Hamiltonian). In fully deterministic systems, RM statistics were conjectured to hold generically for high-lying eigenvalues of

systems with a classical fully chaotic motion. This is the Bohigas–Giannoni–Schmit (BGS) conjecture in quantum chaos [18, 19], supported by many numerical results and by some analytic arguments (see next section). One of the simplest Hamiltonians allowing to test the conjecture, and that will be here employed as a model system, is to consider the motion of a free particle inside a cavity with perfect elastic reflections on the boundary. The upper part of Fig. 1 shows several fully chaotic two–dimensional (2D) examples: the Sinai billiard, the stadium, and the cardioid. The quantization of the motion is given, for a billiard system, by the Schrödinger equation of a free particle with Dirichlet boundary conditions imposed (i.e., the wave function should vanish on the border). In the left part of Fig. 2 is shown the nearest neighbor spacing distribution of high–lying eigenvalues of the cardioid billiard obtained numerically. The cardioid billiard is time–reversal symmetric, and is therefore compared with the ensemble  $\beta = 1$  in Eq. (9) [20].

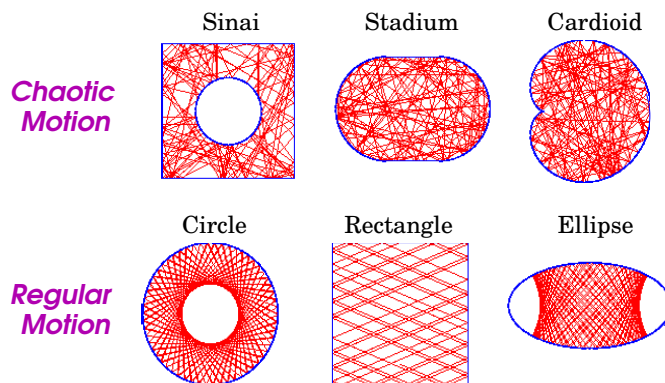


**Fig. 1.** Examples of classical motion inside 2D cavities. Upper part: chaotic, lower part: integrable. In each cavity, a typical trajectory is shown. Taken from [21].

A relevant question is the universality of the ensemble of matrices considered. There is no special reason, aside technical ones, to consider the particular Gaussian distribution of matrix elements described above. Other statistical weights could have been chosen as well. It is therefore important to understand to which extent the results are independent of the distribution. Some form of universality of the local statistics has been shown. As the size of the matrix increases, the bulk eigenvalue distribution converges towards a limit that, to a large extent, is independent of the probability measure used [22, 23].

Through the BGS conjecture, RMT is associated to the concept of complexity, here manifested as chaotic classical motion. In contrast, there are large classes of physical systems where the conjecture does not apply. An extreme and well known class is that of the regular, or integrable, systems.

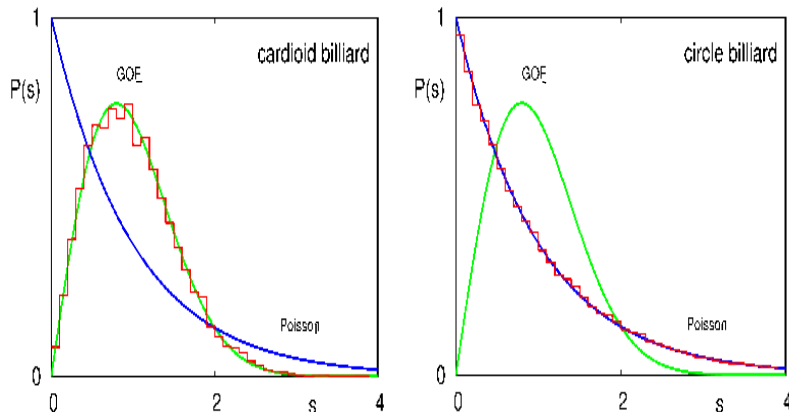


**Fig. 2.** Nearest neighbor spacing distribution for the cardioid and circle billiards, compared to RMT ( $\beta = 1$ ) and Poisson distributions. Taken from [21].

These are systems with as many independent integrals of motion as degrees of freedom. The lower part of Fig. 1 shows several two-dimensional (2D) examples. In the circular billiard, for instance, the two independent integrals of motion are the energy and the angular momentum. The existence of these constants of the motion forces the orbits to form regular patterns, and no exponential sensitivity to perturbations, like in chaotic systems, exists. Regular and fully chaotic motion are two extreme situations. A billiard with an arbitrary shape will generically contain both types of dynamics, regular and chaotic (mixed system). Some aspects of mixed dynamics will be discussed in §5.

When a regular system is quantized, the statistical analysis of the fluctuations give results that are quite different with respect to RMT. What is found is that the local statistics of the corresponding quantum energy levels are described by a Poisson process. (e.g., the eigenvalues behave, statistically, as a set of uncorrelated levels) [24]. Many numerical simulations support this conjecture, though there is no general proof, aside some particular systems [25]. This property is illustrated on the right hand side of Fig. 2, where the nearest neighbor spacing distribution of a circular 2D billiard is compared to the Poisson result,  $p(s) = e^{-s}$  ( $\delta = 1$ ). The form factor of an uncorrelated sequence of levels is independent of  $\tau$ ,

$$K_{unc}(\tau) = \tau_H . \quad (10)$$

In summary, and loosely speaking because there are exceptions that we don't discuss here, for the two types of dynamics considered the local correlations of energy levels are universal and either described by random matrix



theory in chaotic or “complex” systems, or by an uncorrelated Poisson sequence for integrable or “regular” systems.

### 3 Long Range Fluctuations: Semiclassics

In fact, and contrary to what Fig. 2 suggests, RMT or a Poisson process do not describe faithfully the fluctuation properties of real physical systems. The reason is that these simple ensembles fail to describe some important physical features related to the short time dynamics. There is only one time scale that can be associated, through quantum mechanics, to a stationary sequence of random numbers. This is the Heisenberg time, that corresponds to the conjugate time to the mean level spacing. But physical system possess other time scales, that are typically smaller than  $\tau_H$ . In ballistic systems (e.g., no disorder present), like a particle moving freely inside a 2D or 3D cavity, another important time scale is the time of flight across the system, denoted  $\tau_{\min}$ . We will give a precise definition of  $\tau_{\min}$  below using the periodic orbits. This is typically the smallest relevant time scale of a dynamical system. It corresponds to a large energy scale, given by,

$$E_c = h/\tau_{\min} . \quad (11)$$

We will now see that the typical single-particle energy levels of a ballistic dynamical system have, superimposed to the universal local fluctuations on a scale  $\delta$  discussed in the previous section, system-specific long-range modulations on a scale  $E_c$ . These modulations of the density with respect to the average properties of the spectrum are not described by random sequences of numbers (correlated or not).

It turns out that a very convenient tool to analyze in a systematic way the deviations of a quantum spectrum with respect to its average properties is the semiclassical analysis. This method is convenient from either a technical as well as a conceptual point of view, and is justified if a classical limit of the quantum problem exists. This limit can be obtained by different procedures. For example, in the context of nuclear physics it is known that a classical limit of some simple shell models of the nucleus can be obtained by letting the number of particles tend to infinity [26, 27]. More generally, the connexion with a classical dynamics can be done through the mean field, which reduces the fully interacting many-body problem to a single-particle motion in a self-consistent potential. The interest of semiclassical theories is that they offer a unified scheme of analysis, and provide a conceptual framework that allows in many cases to understand a physical property using simple ideas.

The basic object we are interested in is the single-particle density of states

$$\rho(E, x) = g_s \sum_j \delta [E - E_j(x)] . \quad (12)$$

The  $E_j(x)$  are the discrete eigenvalues of the single-particle Hamiltonian  $H$ . The eigenvalues depend on a set of parameters  $x$  that fix, for example, the shape of the potential, or may represent any other external parameter. The prefactor  $g_s$  accounts for spin degeneracy.

The classical motion is described by a function  $H(\mathbf{p}, \mathbf{q})$  of the phase-space variables  $(\mathbf{p}, \mathbf{q})$ . In the semiclassical limit  $\hbar \rightarrow 0$  the quantum density of states can be approximated by a sum of smooth plus oscillatory terms,

$$\rho(E, x) = g_s [\bar{\rho}(E, x) + \tilde{\rho}(E, x)] . \quad (13)$$

The first term is a smooth function of  $E$  that describes the average properties of the spectrum. It is usually known as the Thomas-Fermi contribution (or Weyl expansion for the motion of a particle inside a hard-wall cavity). The leading term of  $\bar{\rho}$  is given by the well-known semiclassical rule that associates, in a  $D$ -dimensional system, a phase-space volume  $h^D$  to each quantum state,

$$\bar{\rho} = \frac{1}{(2\pi\hbar)^D} \int d^D p d^D q \delta(E - H(\mathbf{p}, \mathbf{q})) . \quad (14)$$

Corrections to Eq. (14) depend on derivatives of  $H$  [28]. In the case of the motion inside a 3D cavity, the expansion takes a particularly simple form [29],

$$\bar{\rho} = \frac{V}{4\pi^2} \left( \frac{2m}{\hbar^2} \right)^{3/2} E^{1/2} - \frac{S}{16\pi} \frac{2m}{\hbar^2} + \frac{\mathcal{L}}{16\pi} \left( \frac{2m}{\hbar^2} \right)^{1/2} E^{-1/2} + \mathcal{O}(E^{-3/2}) . \quad (15)$$

Here  $V$  and  $S$  are the volume and the surface of the cavity, and  $\mathcal{L}$  is a typical length that depends on its topology;  $m$  is the mass of the particle. The integral of the density with respect to the energy is also of interest,

$$\mathcal{N}(E, x) = g_s \sum_j \Theta [E - E_j(x)] ; \quad (16)$$

it gives the number of single-particle levels with energy  $E_j \leq E$  (counting function). It can be decomposed as in Eq. (13),

$$\mathcal{N}(E, x) = g_s [\bar{\mathcal{N}}(E, x) + \tilde{\mathcal{N}}(E, x)] . \quad (17)$$

The average part, obtained for a 3D cavity by integrating (15) with respect to  $E$ , is

$$\bar{\mathcal{N}} = \frac{V}{6\pi^2} \left( \frac{2m}{\hbar^2} \right)^{3/2} E^{3/2} - \frac{S}{16\pi} \frac{2m}{\hbar^2} E + \frac{\mathcal{L}}{8\pi} \left( \frac{2m}{\hbar^2} \right)^{1/2} E^{1/2} + \mathcal{O}(1) . \quad (18)$$

Deviations with respect to the smooth behavior of the density are described by the fluctuating part  $\tilde{\rho}$  in Eq. (13). They are given, to leading order in an  $\hbar$ -expansion, by [30, 31],

$$\tilde{\rho}(E, x) = 2 \sum_p \sum_{r=1}^{\infty} A_{p,r}(E, x) \cos [rS_p(E, x)/\hbar + \nu_{p,r}] . \quad (19)$$

The sum is over all the periodic orbits  $p$  of the classical Hamiltonian  $H(\mathbf{p}, \mathbf{q})$ . The index  $r$  takes into account multiple traversals (repetitions) of a primitive orbit  $p$ . The orbits are characterized by their action  $S_p = \oint \mathbf{p} \cdot d\mathbf{q}$ , period  $\tau_p = dS_p/dE$ , stability amplitude  $A_{p,r}$ , and Maslov index  $\nu_{p,r}$ . The functional form of  $A_{p,r}$  depends on the nature of the dynamics. In integrable system, the periodic orbits form continuous families, with all members of a family having the same properties. In contrast, in fully chaotic systems all orbits are unstable and isolated. This important difference is at the origin of the fact, to be discussed in the next sections, that shell corrections are more important in integrable systems than in chaotic ones.

**Note:** Why a sum over periodic orbits? This can be understood from the following simplified argument. The density of states may be calculated from the Green function,  $\rho(E) = -\frac{1}{\pi} \text{Im} \int d^D q \lim_{\epsilon \rightarrow 0^+} G(\mathbf{q}, \mathbf{q}, E + i\epsilon)$ . In the Feynman representation,  $G(\mathbf{q}, \mathbf{q}, E)$  is the propagator for paths of energy  $E$  that start at  $\mathbf{q}$  and come back to  $\mathbf{q}$ . In the limit  $\hbar \rightarrow 0$ , the leading contribution to  $G$  is a sum over all the *classical* trajectories that start and come back to  $\mathbf{q}$ . Finally, a stationary phase approximation of the above integral over  $\mathbf{q}$  selects, among all the classical closed trajectories, those that start and come back to a given point with the same momentum. Those are the periodic orbits.

The fluctuating part  $\tilde{\mathcal{N}}$  of the counting function may be obtained by integration of Eq. (19) with respect to the energy. To leading order in a semiclassical expansion, the integration with respect to the rapidly varying factor  $S_p(E, x)/\hbar$  dominates. This gives, to leading order,

$$\tilde{\mathcal{N}}(E, x) = 2\hbar \sum_p \sum_{r=1}^{\infty} \frac{A_{p,r}}{r\tau_p} \sin [rS_p/\hbar + \nu_{p,r}] . \quad (20)$$

To illustrate the semiclassical approximation of the density of states and of the counting function in a concrete example, we consider the free motion of a spin-1/2 particle inside a three-dimensional (3D) cavity, elastically reflected off the surface. The spherical cavity and the corresponding semiclassical approximation have been extensively studied in the past, and I refer the reader to some of those references for a more detailed presentation [30, 28]. Quantum mechanically, the single-particle energy levels  $E_{n,l}$  of a free particle of mass  $m$  moving inside a cavity of radius  $R$  with Dirichlet boundary conditions are given by the quantization condition,

$$J_{l+1/2}(\sqrt{\epsilon_{n,l}}) = 0 , \quad n = 1, 2, \dots , \quad l = 0, 1, 2, \dots , \quad (21)$$

where  $E_{n,l} = \hbar^2 k_{n,l}^2 / 2m = \hbar^2 \epsilon_{n,l} / 2mR^2 = E_0 \epsilon_{n,l}$ ,  $J$  is the Bessel function, and  $k$  the wavenumber. The previous expressions define the quantities  $\epsilon_{n,l} = (k_{n,l}R)^2$  and  $E_0 = \hbar^2 / 2mR^2$ . The index  $l$  labels the angular momentum of the particle, and  $n$ , that serves to identified the different zeros of  $J_{l+1/2}(\epsilon_{n,l})$

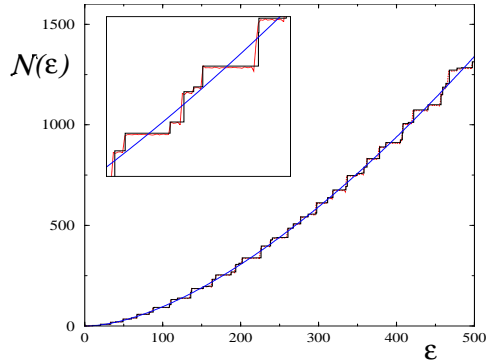


**Fig. 3.** Counting function of a spin-1/2 particle in a 3D spherical cavity. Full staircase: quantum mechanical. Dotted staircase: semiclassical (almost indistinguishable from the quantum mechanical one). Smooth interpolating curve: Weyl's formula. Detail in the inset.

at fixed  $l$ , is the radial principal quantum number. The degeneracy of each quantum mechanical energy level is  $g_{n,l} = 2l + 1$ .

The counting function is defined as,

$$\mathcal{N}_{sph}(\epsilon) = g_s \sum_{n,l} g_{n,l} \Theta(\epsilon - \epsilon_{n,l}) , \quad (22)$$

which increases by a factor  $g_s \times g_{n,l}$  at each eigenvalue  $\epsilon_{n,l}$ . The exact staircase function is represented in Fig. 3 ( $g_s = 2$ ), with the energy measured in units  $\epsilon = E/E_0$ . Big jumps of the function at energy levels with large degeneracies are clearly visible.

We now turn to a semiclassical description of  $\mathcal{N}_{sph}(\epsilon)$ . A classification and discussion of the periodic orbits of the sphere may be found in [30]. Each orbit is characterized by two integers,  $w$  (the winding number), and  $v$  (the number of vertices or bounces of an orbit off the surface) (see Fig. 4). The semiclassical theory leads to an approximate expression of the counting function in terms of these orbits, given by Eqs. (17), (18) and (20). For the sphere, the smooth and oscillatory parts read [30],

$$\overline{\mathcal{N}}_{sph}(\epsilon) = \frac{2}{9\pi} \epsilon^{3/2} - \frac{1}{4} \epsilon + \frac{2}{3\pi} \epsilon^{1/2} , \quad (23)$$

$$\tilde{\mathcal{N}}_{sph}(\epsilon) = -2\sqrt{\epsilon} \sum_{w=1}^{\infty} \sum_{v=2w}^{\infty} \frac{A_{vw}}{\ell_{vw}} \cos(\sqrt{\epsilon} \ell_{vw} + \nu_{vw}\pi/2) . \quad (24)$$

The different factors entering Eq. (24) are defined as,

$$A_{vw} = \begin{cases} -(2\pi w)^{-1} & v = 2w \\ (-1)^w \sin(2\theta_{vw}) \sqrt{\sin(\theta_{vw})/\pi v} \epsilon^{1/4} & v > 2w \end{cases} \quad (25)$$

$$\nu_{vw} = \begin{cases} 0 & v = 2w \\ v + 3/2 & v > 2w \end{cases} \quad (26)$$

$$\ell_{vw} = 2v \cos(\theta_{vw}) \quad (27)$$

$$\theta_{vw} = \pi w/v. \quad (28)$$

The parameter  $\ell_{vw}$  is the length of the periodic orbit  $(v, w)$  of a unit radius sphere, and  $\nu_{vw}$  is the phase attached to each orbit. The semiclassical approximation of  $\mathcal{N}_{sph}$  is also represented in Fig. 3 as a dotted line, together with the average part  $\overline{\mathcal{N}}_{sph}$ . Viewed on large scales, the accuracy of Weyl's formula is quite good. The inset shows a closer view of the function, where the fluctuations with respect to the average and the accuracy of the semiclassical approximation can be appreciated. Orbits with  $w$  up to 40 and  $v$  up to 80 have been used in Eq. (24) to obtain the curve in the figure. It is seen that the semiclassical approximation of  $\mathcal{N}_{sph}$  is quite good.

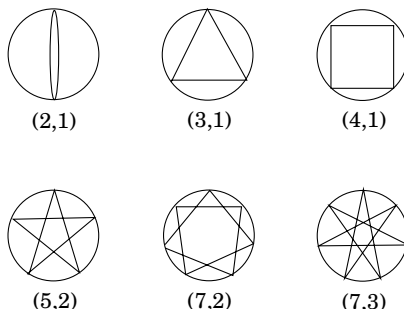


**Fig. 4.** Some of the periodic orbits of the sphere, labeled by  $(v, w)$ , the number of vertices and the number of turns around the center, respectively.

We now let for the moment the spherical cavity and return to general considerations concerning the trace formula. Equation (19) shows that the discrete quantum mechanical spectrum is, formally, recovered from an interferent sum over all the periodic orbits whose contributions add up constructively at the positions of the eigenvalues  $E_j$ , and destructively elsewhere. Since in the vicinity of some reference energy  $E_*$  the action may be expressed as  $S_p(E) \approx S_p(E_*) + \tau_p(E - E_*)$ , each periodic orbit contributes to the density with an oscillatory term, as a function of  $E$ , whose wavelength is  $h/\tau_p$ . Long periodic orbits are therefore responsible for the small scale structures of the spectrum. To resolve the spectrum on an energy scale of the order  $\delta$ , and describe the departures from the average properties on that scale, long periodic orbits of period  $\tau_H$  are needed. In contrast, short orbits describe oscillations of the density of states on large scales. The shortest orbit, of period  $\tau_{\min}$ , defines the outer energy scale  $E_c = h/\tau_{\min}$  of the density

fluctuations. The density modulations on a scale  $E_c$  are usually referred to as shell effects. Their importance heavily depends on the dynamical properties and symmetries of the system. For instance, in systems with a central potential, the angular momentum conservation produce strong degeneracies among eigenvalues. The degeneracies create energy regions where the density of eigenvalues is high compared to the mean, and others where it is small, thus producing long range fluctuations of the density. This is an extreme illustration of level bunching. From a classical point of view, the enhancement produced by symmetries is due to the appearance of families of periodic orbits all having, because of the symmetry, the same action, amplitude, etc. This produces, at the level of the trace formula, an enhancement of the shell effects. However, shell effects are present in arbitrary systems, with or without symmetries, since they are a manifestation of the existence of short periodic orbits, a generic property of any dynamical system. In less symmetric systems they will be less important because the degeneracy of the families of periodic orbits will be lower, or inexistent, like in chaotic systems where periodic orbits are isolated. Correspondingly, the associated shell effects will be less dramatic. This point will be reconsidered in the next sections. See Ref. [3].

The scale  $E_c$  is typically much larger than  $\delta$ . A precise characterization of the difference is given by the adimensional parameter,

$$g = E_c/\delta = \tau_H/\tau_{\min} , \quad (29)$$

which counts the number of single-particle energy levels contained in a shell. It is a measure of the collectivity of the long range spectral modulations imposed by the shortest periodic orbits. It will play an important role when quantifying the difference of size of shell effects in regular and chaotic systems. Denoting  $L = V^{1/3}$  the typical size of the system, it follows from Weyl's law for a D-dimensional cavity that  $g$  is proportional to  $(kL)^{D-1}$ , where  $k$  is the wavenumber at energy  $E$ . Thus, in the semiclassical regime of short wavelength compared to the system size,  $kL \gg 1$ , the parameter  $g$  is large.

To have a more precise idea of the consequences of the presence of an outer scale in the oscillatory structure of the density, and of its relation with the universal properties discussed in §2, consider again the form factor. Using the semiclassical approximation of the density, Eq. (19), it can be shown [32] that  $K(\tau)$  is expressed as,

$$K(\tau) = h^2 \left\langle \sum_{p,p'} \sum_{r,r'} A_{p,r} A_{p',r'} \cos \left( \frac{rS_p - r'S_{p'}}{\hbar} \right) \delta \left[ \tau - \frac{(r\tau_p + r'\tau_{p'})}{2} \right] \right\rangle_E , \quad (30)$$

where the brackets indicate an energy average (see §4.2 for a more precise characterization of the averaging window).

For times  $\tau \ll \tau_H$  the off-diagonal contributions  $p \neq p'$  in Eq. (30) are eliminated by the averaging procedure, and the behavior of  $K(\tau)$  is well described by the diagonal terms  $p = p'$ . This gives a series of delta peaks at

$$\tau = \tau_p,$$

$$K(\tau) \approx h^2 \sum_{p,r} A_{p,r}^2 \delta(\tau - r\tau_p) . \quad (31)$$

The lowest peak is located at  $\tau = \tau_{min}$ , and for  $\tau \leq \tau_{min}$  the form factor is identically zero. Since the position and amplitude of this peaks are system dependent, it follows that for times of the order of  $\tau_{min}$  no statistical universal behavior of the form factor exists, and Eqs. (8) and (10) do not provide a good description. In particular, the fact that  $K(\tau) = 0$  for  $\tau \leq \tau_{min}$  is completely out of reach of the models based on random sequences.

Going to longer times, but still remaining in the regime of validity of the diagonal approximation,  $\tau_{min} \ll \tau \ll \tau_H$ , it can be shown that indeed the RMT behavior (8) in chaotic systems, and the uncorrelated statistics (10) in integrable systems, are recovered. Their semiclassical origin is related to the statistical behavior of long classical periodic orbits [33, 32]. There is no proof of the agreement for longer times, aside some additional corrections in the  $\tau$  expansion of the form factor in time-reversal chaotic systems [34], and results in some particular integrable models (e.g., the rectangular billiard, see [25]). We will therefore simply assume that for times  $\tau \gg \tau_{min}$  the statistical description of the previous section, based on random sequences, holds. Figure 5 summarizes the main features of the form factor for integrable and chaotic systems.

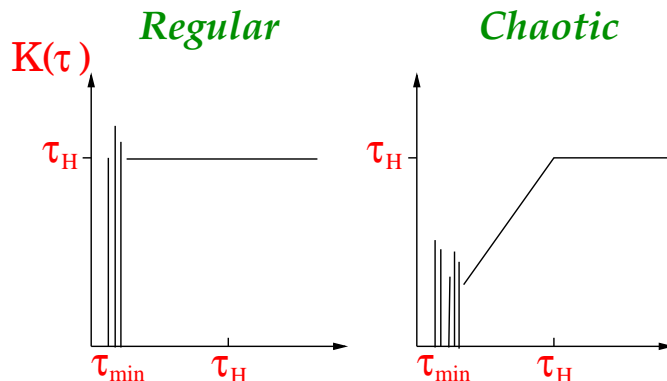


**Fig. 5.** Schematic view of the form factor for regular and chaotic systems

In summary: the fluctuations of the single-particle spectrum in ballistic systems are schematically of two types. On scales of order  $\delta$ , they are universal (described by an uncorrelated sequence for integrable systems, and by RMT in chaotic ones), as discussed in the previous section. In contrast, on scales of order  $E_c = g\delta$ , with  $g \gg 1$ , there are long range modulations whose structure and amplitude are system specific.

## 4 Fermi Gas

We now turn to the central theme of these lectures, the theory of the quantum fluctuations in interacting Fermionic systems. Our reference model will be a confined Fermi gas, i.e. a gas of non-interacting particles moving in a self-consistent mean field. It turns out, as it will be discussed below, that such an approximation is well justified when studying the thermodynamic fluctuations of interacting systems like the atomic nucleus or the valence electrons in metals.

The starting point is a grand-canonical description, appropriate to study the properties of an open system. Although this choice is in part motivated by technical reasons, we will specify how to adapt the results to other physical situations. In particular, to systems where the number of particles is conserved, like the atomic nucleus.

When the chemical potential  $\mu$  is fixed, the thermodynamic behavior of a Fermi gas is described by the grand potential,

$$\begin{aligned} \Omega(\mu, T, x) &= -k_B T \int dE \rho(E, x) \log[1 + e^{(\mu-E)/k_B T}] \\ &= - \int dE \mathcal{N}(E, x) f(E, \mu, T) , \end{aligned} \quad (32)$$

where  $\rho(E, x)$  and  $\mathcal{N}(E, x)$  are the single-particle density of states and the counting function, respectively, already introduced in §3.  $T$  is the temperature, and  $k_B$  is Boltzmann's constant.  $x$  parametrizes the mean field potential, or represents some additional external parameter, and  $f$  is the Fermi function

$$f(E, \mu, T) = \frac{1}{1 + e^{(E-\mu)/k_B T}} . \quad (33)$$

When the number of particles  $A$  in the gas is fixed, the energy of the system is

$$U(A, T, x) = \int dE E \rho(E, x) f(E, \mu, T) , \quad (34)$$

where  $\mu$  is determined from the equation

$$A = \int dE \rho(E, x) f(E, \mu, T) . \quad (35)$$

Knowing these two thermodynamic potentials, other thermodynamic functions are directly obtained by differentiation with respect to  $\mu$ ,  $x$ , or  $T$ .

### 4.1 Semiclassical approximation

We now exploit the semiclassical expansion of the density of states to obtain semiclassical expressions for the thermodynamic functions of the gas. Using



Eq. (13), the density of states in Eq. (32) is written as a sum of smooth plus oscillatory terms. This approximation is valid in the semiclassical regime  $A \gg 1$  where the typical wavelength of the fermions at energy  $\mu$  is much smaller than the system size, and is less accurate at the bottom of the spectrum.

The substitution in Eqs. (32) and (34) of the density of states by its average behavior, Eq. (14) or (15), gives rise to the smooth, bulk classical expressions for the thermodynamics of the Fermi gas [35]. In finite fermionic systems, like the atomic nucleus or the electron gas in a metallic particle, it is however well known that the smooth part of the thermodynamic properties of the interacting system are not correctly described by the Fermi gas approximation. In contrast, and this is a crucial point, it is known that the *fluctuations* of the properties of the interacting system with respect to the average behavior and, in particular, the energy fluctuations, are well approximated by the fluctuations of the Fermi gas. This is the content of the Strutinsky energy theorem [36]. This property justifies, in interacting many-body Fermionic systems, the validity of the analysis of the fluctuations presented here, based on a single-particle mean-field picture.

Equation (19) is then inserted in Eq. (32) to compute the oscillatory part of the grand potential. To leading order in  $\hbar$  and for low temperatures ( $k_B T \ll \mu$ , degenerate gas approximation) the integral gives [6],

$$\tilde{\Omega}(\mu, T, x) = 2\hbar^2 g_s \sum_p \sum_{r=1}^{\infty} \frac{A_{p,r} \kappa_T(r \tau_p)}{r^2 \tau_p^2} \cos(rS_p/\hbar + \nu_{p,r}) . \quad (36)$$

In this expression, all the classical orbits have energy  $E = \mu$ , and they all depend on the external parameter  $x$ . The temperature introduces the prefactor  $\kappa_T(\tau)$ ,

$$\kappa_T(\tau) = \frac{\tau/\tau_T}{\sinh(\tau/\tau_T)} , \quad \tau_T = h/(2\pi^2 k_B T) . \quad (37)$$

This factor acts as an exponential cut off for orbits with period  $\tau_p > \tau_T$ . For temperatures such that  $\tau_{min} \gg \tau_T$ , the quantum fluctuations are washed out and only the smooth part of  $\Omega$  given by  $\bar{\rho}$  survives.

Similarly we may analyze the energy of the gas at a fixed number of particles. The main technical difficulty here is that  $\mu$  is not constant as some external parameter is varied (like the shape of the nucleus for example), but varies in order to satisfy, at any  $x$ , the condition (35) ( $\mu$  is in fact a function of  $A$ ,  $T$ , and  $x$ ). It should therefore also be decomposed into smooth and oscillatory parts,

$$\mu = \bar{\mu} + \tilde{\mu} , \quad (38)$$

with  $\bar{\mu}$  defined by the condition

$$A = \int dE \bar{\rho}(E, x) f(E, \bar{\mu}, T) . \quad (39)$$

The fluctuating part of the energy of the system is defined as

$$\tilde{U} = \int dE E \rho(E) f(E, \mu, T) - \int dE E \bar{\rho}(E) f(E, \bar{\mu}, T) . \quad (40)$$

Using Eq. (13), assuming that  $\tilde{\mu} \ll \bar{\mu}$ , and integrating by parts Eq. (40), one finds,

$$\tilde{U} = \int dE E \rho(E) f'_{\tilde{\mu}}(E, \bar{\mu}, T) \tilde{\mu} - \int dE \tilde{N}(E) f(E, \bar{\mu}, T) - \int dE E \tilde{N}(E) f'_E(E, \bar{\mu}, T) , \quad (41)$$

where  $f'_{\tilde{\mu}}(E, \bar{\mu}, T) = df(E, \bar{\mu}, T)/d\tilde{\mu}$  and  $f'_E(E, \bar{\mu}, T) = df(E, \bar{\mu}, T)/dE$ . From Eqs. (35) and (39), in a similar approximation, it follows that

$$\int dE E \rho(E) f'_{\tilde{\mu}}(E, \bar{\mu}, T) \tilde{\mu} = \int dE E \tilde{N}(E) f'_E(E, \bar{\mu}, T) .$$

This implies,

$$\tilde{U}(A, T, x) = - \int dE \tilde{N}(E, x) f(E, \bar{\mu}, T) . \quad (42)$$

Comparing this equation with Eq. (32), we conclude that the fluctuations of the energy at a fixed number of particles  $A$  coincide, to leading order in an expansion in terms of  $\tilde{\mu}$ , with the fluctuations of  $\Omega$  evaluated at a chemical potential  $\bar{\mu}(A, T, x)$  defined by inverting Eq. (39). From Eq. (36), we therefore get,

$$\tilde{U}(A, T, x) = 2\hbar^2 g_s \sum_p \sum_{r=1}^{\infty} \frac{A_{p,r} \kappa_T(r \tau_p)}{r^2 \tau_p^2} \cos(rS_p/\hbar + \nu_{p,r}) . \quad (43)$$

All the classical orbits that enter this expression are at energy  $\bar{\mu}(A, T, x)$ .

$\tilde{U}$  are the variations of the energy due to kinematic effects ("dynamical fluctuations"). Equation (43) is the main theoretical tool to analyse its properties. It associates to each periodic orbit a certain amount of energy that depends on its period, stability, etc. The total contribution is the sum of all the energies associated to the periodic orbits. The temperature enters only through the prefactor  $\kappa_T$ , whose magnitude decreases as  $T$  increases. For studying the contribution of kinematic effects to the mass of the nuclei, we simply take  $T = 0$ . Then  $\kappa_T = 1$ , and Eq. (43) becomes,

$$\tilde{\mathcal{B}}(A, x) = 2\hbar^2 g_s \sum_p \sum_{r=1}^{\infty} \frac{A_{p,r}}{r^2 \tau_p^2} \cos(rS_p/\hbar + \nu_{p,r}) . \quad (44)$$

This equation describes the fluctuations of the mass due to dynamical effects; they are added on top of the smooth part given by the von Weizsäcker formula. At  $T = 0$ ,  $\mu$  is the Fermi energy  $E_F$  of the system, which is also decomposed into a smooth and an oscillatory part,  $E_F = \bar{E}_F + \tilde{E}_F$ . The definition of the smooth part of the Fermi energy is, from Eq. (39) at  $T = 0$ , given by

$$A = \int^{E_F} dE \rho(E, x) = \int^{\bar{E}_F} dE \bar{\rho}(E, x) = \bar{\mathcal{N}}(\bar{E}_F, x) , \quad (45)$$

which defines, by inversion, the function  $\bar{E}_F(A, x)$ . All the classical orbits in Eq. (44) are evaluated at energy  $\bar{E}_F(A, x)$ .

The oscillatory part of other thermodynamic functions may be computed by direct differentiation of  $\tilde{\Omega}$  or  $\tilde{U}$  with respect to the appropriate parameter [6].

## 4.2 Statistical Analysis of the Fluctuations

Equation (44) requires the knowledge of the periodic orbits and of their different properties (period, stability, Maslov index, etc) in order to compute the fluctuating part of the mass. In this Section, instead of a detailed computation and description of the fluctuations for a particular system, based on a precise knowledge of some set of periodic orbits, the aim is to study their statistical properties. The interest of such an approach is well known: using a minimum amount of information, a statistical analysis allows to establish a classification scheme among the fluctuations of different physical systems. It also allows to distinguish the generic from the specific, and provides a powerful predictive tool in complex systems. A general description of the statistical properties of the quantum fluctuations of thermodynamic functions of integrable and chaotic ballistic Fermi gases, and of their temperature dependence, was developed in Ref. [6]. Here we will only concentrate on the energy of the gas at zero temperature, e.g., its mass.

The fluctuating part  $\tilde{\mathcal{B}}(A, x)$  shows, as a function of the number of particles or, alternatively, the Fermi energy  $\bar{E}_F$ , oscillations described by Eq. (44). The statistical properties of  $\tilde{\mathcal{B}}$ , and in particular its probability distribution, are computed in a given interval of size  $\Delta\bar{E}_F$  around  $\bar{E}_F$ . This interval must satisfy two conditions. It must be sufficiently small in order that all the classical properties of the system remain almost constant. This is fulfilled if  $\Delta\bar{E}_F \ll \bar{E}_F$ . Moreover, it must contain a sufficiently large number of oscillations to guarantee the convergence of the statistics. As stated previously the largest scale associated to the oscillations is  $E_c$ . Then clearly we must have  $\Delta\bar{E}_F \gg E_c$ . In the semiclassical regime the hierarchical ordering between the different scales is therefore

$$\delta \ll E_c \ll \Delta\bar{E}_F \ll \bar{E}_F .$$

## Second Moment and Universality

The average value of the fluctuating part  $\tilde{\mathcal{B}}$  defined as in Eq. (44) is zero. This is not strictly true in general, because it is possible to show that subleading corrections in the expansion (42) have a non-zero average. Ignoring this, the variance is the more basic aspect of the probability distribution of the

fluctuations. It provides the typical size of the oscillations, and can easily be compared with experiments. We will now compute a general expression for the second moment of the probability distribution, that allows also to make an analysis of the universal properties of the fluctuations. The key point is to understand which orbits give the dominant contribution in Eq. (44). Though it is clear that the weight of an individual orbit decreases with its period, the net result of the sum of the contributions is unclear, because the number of periodic orbits of a given period grows with the period.

From Eq. (44) the square of  $\tilde{\mathcal{B}}$  is expressed as a double sum over the periodic orbits involving the product of two cosine. The latter product may be expressed as one half the sum of the cosine of the sum and that of the difference of the actions. The average over the term containing the sum of the actions vanishes, due to its rapid oscillations on a scale  $\Delta\bar{E}_F$ . Therefore, letting aside for the moment the spin factor (which will be discussed later on),

$$\langle \tilde{\mathcal{B}}^2 \rangle = 2 \hbar^4 \left\langle \sum_{p,p'} \sum_{r,r'} \frac{A_{p,r}}{r^2 \tau_p^2} \frac{A_{p',r'}}{r'^2 \tau_{p'}^2} \cos \left( \frac{S_p - S_{p'}}{\hbar} \right) \right\rangle_{\bar{E}_F, x}. \quad (46)$$

To simplify the notation we have included the Maslov indices in the definition of the action. Ordering the orbits by their period, and taking into account the restrictions imposed by the averaging procedure, the variance Eq. (46) can be related to the semiclassical definition of the form factor  $K(\tau)$ , Eq. (30). The variance of the mass fluctuations takes the simple form [6, 7],

$$\langle \tilde{\mathcal{B}}^2 \rangle = \frac{\hbar^2}{2\pi^2} \int_0^\infty \frac{d\tau}{\tau^4} K(\tau). \quad (47)$$

Analogous expressions connecting the variance of different thermodynamic quantities, like for example the response of the gas to a perturbation, the entropy, etc, at any temperature, can be found in Ref. [6].

To obtain Eq. (47) we made use of the fact that the orbits giving a non-zero contribution to (46) have similar actions (unless their average will be zero). This implies that their period is also similar, and can be considered to be the same in the prefactor (but not in the argument of the oscillating part).

Based in Eq. (47) we now make a simple analysis of the variance of the mass fluctuations. From Eqs. (7) and (8) it follows that for chaotic systems the integrand in Eq. (47) behaves as  $\tau^{-3}$  for short times and  $\tau^{-4}$  for long times, while Eq. (10) implies that for integrable motion the integrand varies as  $\tau^{-4}$ . Therefore in both cases the integral (47) converges for long times. The dominant contributions come from short times, where the integrand is large. If the form factor of a pure random sequence is used in Eq. (47), the integral diverges. In real systems the divergence of the integral is in fact stopped by the cutoff at  $\tau = \tau_{min}$  of the form factor. Because, as shown in §3, the short-time structure of the form factor is specific to each system (i.e.,

it is not universal), we see from Eq. (47) that in general the second moment of the mass fluctuations is non-universal, and consequently the same is true for the probability distribution.

We thus conclude that *the fluctuations of the mass are, regardless of the regular or chaotic nature of the motion, dominated by the short non-universal periodic orbits of the system.*

It should be mentioned that this is a particular property of the mass, that is non generic, and therefore not shared by all other thermodynamic functions. It can be shown that the fluctuations of some functions, like the entropy for example, are dominated at low temperatures by times much larger than  $\tau_{\min}$ ; the corresponding distributions are universal. For a given function, the universality can also depend on the nature of the dynamics. See Ref. [6].

### 4.3 The second moment in the $\tau_{\min}$ -approximation

We have demonstrated that the main contributions to the dynamical part of the mass come from the shortest periodic orbits. On the other hand, we have seen in §3 that for short times a good approximation to the form factor (30) is to keep only the diagonal terms in the double sum over the periodic orbits, Eq. (31). Using the latter approximation, the variance of the fluctuations of the mass is expressed as,

$$\langle \tilde{B}^2 \rangle \approx 2 \hbar^4 \sum_{p,r} \frac{A_{p,r}^2}{r^4 \tau_p^4}. \quad (48)$$

This expression requires the explicit knowledge of the periodic orbits. This information is not always available, like for example in the case of the atomic nucleus. There is, however, a simple way to estimate the variance that requires a minimum amount of information on the orbits. The approximation consists in using in Eq. (47) the corresponding form factor (of an uncorrelated sequence given by Eq. (10) for a regular dynamics, of RMT given by Eq. (7) for a chaotic motion), and to impose the additional and important condition  $K(\tau) = 0$  for  $\tau < \tau_{\min}$  in all cases. This is clearly an approximation, that we call the  $\tau_{\min}$ -approximation. It extrapolates the statistical behavior of the orbits down to times  $\tau \approx \tau_{\min}$ , ignoring the short-time system-dependent structures. All the short-time structures are condensed into a single parameter, the period of the shortest orbit.

The virtue of the  $\tau_{\min}$ -approximation is to provide a simple estimate of the size of the fluctuations, as well as of its dependence with the number of particles, using a minimum amount of information.

Since the integral obtained from Eq. (47) in the  $\tau_{\min}$ -approximation is straightforward, we do not give here a detailed account of its computation. The result, for integrable and chaotic systems, given as an expansion in terms of the small parameter  $1/g$ , is,

$$\langle \tilde{\mathcal{B}}^2 \rangle = \begin{cases} \frac{1}{24\pi^4} g E_c^2 & \text{Integrable} \\ \frac{1}{8\pi^4} E_c^2 \left( 1 - \frac{2}{g} + \mathcal{O}(g^{-2} \log g) \right) & \text{Chaotic } \beta = 1 \\ \frac{1}{16\pi^4} E_c^2 \left( 1 - \frac{1}{3g^2} \right) & \text{Chaotic } \beta = 2 . \end{cases} \quad (49)$$

It is evident from these expressions that the fundamental energy scale that determines the energy fluctuations is  $E_c$ , and not  $\delta$ , or  $\overline{E}_F$ . This is natural, since we have shown that the energy or mass fluctuations are controlled by the long-range fluctuations of the single-particle spectrum produced by the short orbits on a scale  $E_c$ . Fluctuations of the levels in smaller energy scales, whose statistical properties are universal as discussed in §2, contribute with  $1/g$  corrections in Eq. (49). In chaotic systems the variance of the fluctuations is twice smaller in systems without time reversal symmetry. Semiclassically, this is also easy to understand, because in systems with time reversal symmetry each orbit is doubly degenerate (the primitive one and its time-reversed), in contrast to systems with no time reversal symmetry. The coherent contribution of these pairs of orbits produces a variance twice larger for  $\beta = 1$ . Finally, the variance of the fluctuations is  $g$ -times larger in integrable systems compared to chaotic ones. This amplification, which could be quite large (a precise estimate for nuclei is given in the next section), has as semiclassical origin the existence of families of periodic orbits all contributing in phase in Eq. (43). This estimate is valid for generic integrable systems. Even larger amplifications could exist in “super-integrable” systems (cf next section).

Higher moments of the probability distribution of the energy fluctuations may be computed similarly. Starting from Eq. (44), a generalization of the diagonal approximation used for the second moment can be implemented [6]. The results show that the moments of the distribution are generically all different from zero, giving rise to asymmetric probability distributions. For example, the third moment is given by,

$$\langle \tilde{\mathcal{B}}^3 \rangle \approx 6 \hbar^6 \sum_p \sum_{r_1=1}^{\infty} \sum_{r_2=1}^{\infty} \mathcal{A}_{p,r_1} \mathcal{A}_{p,r_2} \mathcal{A}_{p,r_1+r_2} \cos(\nu_{p,r_1} + \nu_{p,r_2} - \nu_{p,r_1+r_2}) , \quad (50)$$

where  $\mathcal{A}_{p,r} = A_{p,r}/r^2 \tau_p^2$ . This and the corresponding expressions for higher moments were explicitly tested in some integrable and chaotic models, where it is found that they work extremely well [6, 8, 9].

## 5 Nuclear Masses

The binding energy of a nucleus is defined by Eq. (1). It is a direct measure of the cohesion and stability of a nucleus. It is customary, as was done in the

previous sections, to analyze the experimental values observed by decomposing  $\mathcal{B}$  into two parts,

$$\mathcal{B}(E, x) = \bar{\mathcal{B}}(E, x) - \tilde{\mathcal{B}}(E, x) . \quad (51)$$

This splitting is at the basis of the so-called shell correction method, introduced in nuclear physics by Strutinsky [37] (see also [3, 38]). Note the minus sign we have introduced in front of  $\tilde{\mathcal{B}}$ . The average part of  $\mathcal{B}$  is described by a liquid drop model à la von Weizsäcker,

$$\bar{\mathcal{B}} = a_v A - a_s A^{2/3} - a_c \frac{Z^2}{A^{1/3}} - a_A \frac{(N - Z)^2}{A} - a_p \frac{t_1}{A^{1/2}} . \quad (52)$$

The different terms in this expansion are associated to volume effects, surface effects, Coulomb interaction, proton–neutron asymmetries, and pairing effects, respectively.  $N$  and  $Z$  are the number of neutrons and protons,  $A = N + Z$  is the total nucleon number, and  $t_1 = -1, 0, +1$  for even–even, odd–even, and odd–odd nuclei, respectively. Note that all the terms are smooth functions of  $A$ ,  $N$ , and  $Z$ , except  $t_1$  that takes into account odd–even effects.

In contrast to  $\bar{\mathcal{B}}$ , the oscillating energy  $\tilde{\mathcal{B}}$ , that describes deviations with respect to the smooth part, can be analyzed, to leading order in a one–body density expansion, in terms of the fluctuations computed from a single–particle spectrum. This is the content of the Strutinsky energy theorem [36]. As explained in §4, this contribution is related to kinematic aspects of the nucleus. It contains explicit information about the motion of the nucleons in the self–consistent mean field. The net output of the semiclassical theory for the oscillatory part of the binding energy is Eq. (44), that expresses  $\tilde{\mathcal{B}}$  as a sum of contributions, each depending on a classical periodic orbit of the mean–field potential. Our purpose now is to explicitly investigate the ability of such a formula to describe the experimentally measured masses of the atomic nuclei.

In order to proceed, the first thing to do is to subtract from the experimental data the average part  $\bar{\mathcal{B}}$ . If this is done from the 1888 nuclei with  $Z, N \geq 8$  of the 1995 Audi–Wapstra compilation [39], the result is Fig. 6. The difference  $\tilde{\mathcal{B}} = \bar{\mathcal{B}} - \mathcal{B}$  is plotted as a function of the neutron number (top part). Each point in the figure represents a nucleus. The parametrization of  $\bar{\mathcal{B}}$  used is taken from Ref. [40]:  $a_v = 15.67$ ,  $a_s = 17.23$ ,  $a_A = 23.29$ ,  $a_c = 0.714$ , and  $a_p = 11.2$  (all in MeV).

A clear oscillatory structure (the shells) of amplitude  $\sim 15$  MeV is observed, with well defined sharp minima, that contrast with the more smooth and rounded shape of the maxima. Another peculiar feature of the shells is that the wavelength of the oscillations clearly increases with  $N$ . A minimum in this plot corresponds to a minimum of  $\tilde{\mathcal{B}}$  (and therefore, locally, to a maximum of  $\mathcal{B}$ ). It defines more stable nuclei. The minima are located at the "magic" numbers  $N = 2, 8, 20, 28, 50, 82, 126$  ( $N = 8$  and  $20$  are not

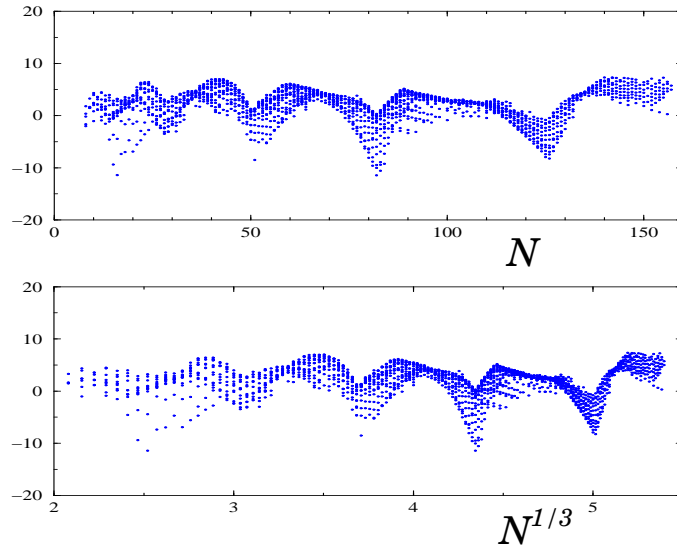


**Fig. 6.** The mass difference  $\tilde{\mathcal{B}} = \bar{\mathcal{B}} - \mathcal{B}$  (in MeV) for the 1888 nuclei of the 1995 Audi–Wapstra compilation. Top: as a function of the neutron number  $N$ . Bottom: as a function of  $N^{1/3}$ .

clearly visible in this figure). The usual interpretation of these minima is in terms of the existence of large gaps in the single–particle spectrum. However, this definition is ill–defined, the notion of a large gap being ambiguous. In the following, we will see that the most natural and simple interpretation of all the characteristic features of this figure, including the position of the magic numbers, is in terms of the periodic orbits of the mean–field potential. This simple description does not pretend to be a substitute of more elaborated many–body calculations. However, the semiclassical theory clearly does something very important: it grasps the essence of the physical mechanism responsible for the oscillatory structure of the nuclear masses, and therefore provides a basic tool towards a general understanding of shell effects.

### 5.1 Regular motion: the spheroidal cavity

To develop a semi–quantitative theory to explain the main features of Fig. 6, a particular model needs to be specified. In the mean–field approach adopted here, what is required is the shape of the mean–field potential. Before selecting one, we need to make some general considerations to guide our choices. In its ground state, the nucleus is minimizing its mass (and therefore maximizing  $\mathcal{B}$ ). The shell corrections are an important component of the extremization procedure since, locally, they control it. The type of dynamics the nucleons are undergoing depends on the form of the mean field potential, through the parameter  $x$ . The function  $\mathcal{B}(A, x)$  has to be maximized with respect to  $x$



at a fixed number of particles. Which type of dynamics is energetically more favorable? As we have seen in §4, the amplitude of the shell effects is more important when the motion of the nucleons is regular, by a factor  $\sqrt{g}$ , as compared to a chaotic dynamics. To obtain a  $\tilde{\mathcal{B}}$  as large, and negative, as possible, a mean field that produces a regular motion is therefore preferable.

For the mean-field approach and the semiclassical techniques employed here to be meaningful, a large number of nucleons is required. In that case, experiments show that a good approximation to the mean field is a potential of the Wood-Saxon type, i.e., relatively flat in the interior of the nucleus and steep on the surface [2]. To simplify, we will consider the potential to be strictly flat in the interior (and set, by convention, to zero), and infinite at the border. Our schematic model of the nucleus will therefore be a mean-field potential given by a cavity, or billiard, with hard walls: the nucleons freely move at the interior, and are elastically scattered off the walls. The simplest geometry that produces a regular motion of the nucleons, and that is of clear interest in nuclear physics, is a spherical cavity. We will therefore start by considering in some detail the mass fluctuations of a Fermi gas located at the interior of a 3D spherical cavity.

Quantum mechanically, at  $T = 0$  the fluctuating part of the energy of a Fermi gas of  $A$  particles in a spherical cavity of radius  $R$  is given by,

$$\tilde{\mathcal{B}}_{sph} = \frac{\bar{E}_F}{\epsilon_F} \sum_{n,l} \epsilon_{n,l} - \bar{\mathcal{B}}_{sph} . \quad (53)$$

The normalized single-particle energies  $\epsilon_{n,l}$  were defined in §3. The average part of the binding energy is given by  $\bar{\mathcal{B}}_{sph} = g_s(\bar{E}_F/\epsilon_F)[(2/15\pi)\epsilon_F^{5/2} - (1/8)\epsilon_F^2 + (2/9\pi)\epsilon_F^{3/2}]$ . The sum in Eq. (53) is made over the lowest  $A$  states of the sphere, taking into account the spin ( $g_s = 2$ ) as well as the intrinsic ( $g_{n,l} = 2l + 1$ ) degeneracies. The energy factor in front of the sum is written, for convenience,  $\bar{E}_F/\epsilon_F = \hbar^2/2mR^2 = E_0$ , where

$$\epsilon_F = (\bar{k}_F R)^2 = \bar{E}_F/E_0 , \quad (54)$$

$\bar{E}_F = \hbar^2 \bar{k}_F^2/2m$  is the average Fermi energy, and  $m$  is the nucleon mass. Note that the normalized energy  $\epsilon_F$  is equivalent, up to a constant factor, to the adimensional shell parameter  $g$ . Indeed, for a 3D cavity  $g$  is written, for  $A \gg 1$ ,

$$g = \frac{g_s}{\pi} \frac{V \bar{k}_F^2}{\ell_{min}} ,$$

where  $\ell_{min}$  is the length of the shortest periodic orbit. For a sphere, with  $V = (4/3)\pi R^3$  and  $\ell_{min} = 4R$ , this gives,

$$g = \frac{g_s}{3} (\bar{k}_F R)^2 = \frac{g_s}{3} \epsilon_F .$$

Semiclassically, the fluctuating part of the binding energy of the Fermi gas is given by Eqs. (44) and (45). The former is obtained by integrating

with respect to the energy up to  $\bar{E}_F(A, x)$  the oscillating part of the counting function. For a spherical cavity,  $\tilde{\mathcal{N}}$  is given by Eq. (24). As usual, and to leading order in a semiclassical expansion, only the integration with respect to the rapidly varying phase factors is kept in the integral. As a result, the oscillatory part of the binding energy of a Fermi gas in a 3D spherical cavity is,

$$\tilde{\mathcal{B}}_{sph}(A, x) = 4 \bar{E}_F g_s \sum_{w=1}^{\infty} \sum_{v=2w}^{\infty} \frac{A_{vw}}{\ell_{vw}^2} \sin(\bar{k}_F R \ell_{vw} + \nu_{vw} \pi/2) . \quad (55)$$

$A_{vw}$ ,  $\ell_{vw}$ , and  $\nu_{vw}$  were defined in Eqs. (25)–(28). In  $A_{vw}$ , the rescaled energy  $\epsilon$  has to be replaced by the rescaled Fermi energy  $\epsilon_F$ .

For simplicity, we consider separately the contributions to the binding energy of the neutrons and of the protons. The contribution of the neutrons is given by Eq. (55) putting  $A = N$ . If the energy of the Fermi gas with a spherical shape is computed as a function of the Fermi energy (grand-canonical ensemble), it is found that the semiclassical approximation to the exact result gives a very accurate description, of a quality comparable to what was obtained in §3 for the counting function (cf Fig. 3). The aim here, however, is to compute  $\tilde{\mathcal{B}}$  as a function of the neutron number. The dependence of  $\bar{E}_F$  (or of  $\epsilon_F$ ) on  $N$  is given, according to Eq. (45), by the inversion of the smooth part of the counting function. From Eqs. (17) and (23), the equation to invert is,

$$\frac{N}{g_s} = \frac{2}{9\pi} \epsilon_F^{3/2} - \frac{1}{4} \epsilon_F + \frac{2}{3\pi} \epsilon_F^{1/2} . \quad (56)$$

When the number of nucleons is large, only the first term in the r.h.s. of Eq. (56) may be kept. Then,

$$\bar{k}_F R = \sqrt{\epsilon_F} = \left( \frac{9\pi}{2g_s} N \right)^{1/3} = 1.92 N^{1/3} , \quad (57)$$

where we used  $g_s = 2$ , the spin degeneracy. From Eq. (54), the corresponding Fermi energy is,

$$\bar{E}_F = \frac{\hbar^2}{2mR^2} \epsilon_F = 1.16 \frac{\hbar^2}{mr_0^2} = 40 \text{ MeV} , \quad (58)$$

where we set the nuclear radius to  $R = r_0 A^{1/3}$ ,  $r_0 = 1.1$  fm, and  $m = 939$  MeV. We have moreover assumed, for simplicity, an equal number of protons and neutrons,  $A = 2N = 2Z$ .

Equation (57) has a very simple and important consequence on the shell oscillations. The oscillating part of the binding energy is given by a sum of interferent terms each having, according to Eqs. (55) and (57), a phase factor proportional to  $N^{1/3}$ . As a function of  $N$ ,  $\tilde{\mathcal{B}}_{sph}$  will therefore present oscillations whose wavelength grows as  $N^{2/3}$ . Alternatively, a plot of the nuclear

binding energy as a function of  $N^{1/3}$ , instead of  $N$ , must show constant-wavelength oscillations. This fact is confirmed, for the experimental data, in the bottom part of Fig. 6.

To obtain a good semiclassical description of the shell effects it is not enough to keep only the first term in the r.h.s. of Eq. (56). The full equation should be used to compute  $\epsilon_F$  as a function of  $N$  (this is particularly important for the phase factors  $\bar{k}_F R$  in Eq. (55), and less for the prefactors). When this is done, a qualitative agreement between the exact and the semiclassical results for the energy of a Fermi gas on a sphere is obtained (see Fig. 12 in Ref. [41]). The precision is however not satisfactory, and clear deviations between the exact and semiclassical results are still observed. This is due to the intrinsic difficulty of computing accurately the Fermi energy as a function of the number of particles. The problem is particularly difficult (and probably one of the worst cases that can be found) for the sphere, where large degeneracies are present. These degeneracies make the function  $E_F(N, x)$ , defined by inverting  $N = \int^{E_F} \rho(E, x) dE$ , ill defined.

There are different ways to cure this problem. A first possibility is to take into account higher order terms in the expansion (42) in terms of  $\tilde{\mu}$ . The other method is to directly compute (numerically) the integral in Eq. (40), as was done in Ref. [41]. In this way, good agreement between the quantum mechanical and the semiclassical results for the sphere is obtained. This is the method employed here to compute semiclassically the binding energies, shown in the figures below, as a function of  $N$ . We will continue, however, to refer to the less accurate (but qualitatively correct and more tractable) approximation (55) for general considerations and discussions.

A priori, there are no adjustable parameters in the model. In particular, the value of  $\bar{k}_F R$  is determined, for a given number of neutrons, by Eq. (56). However, we find that a better agreement with the experimental data is obtained if the value of the constant in Eq. (57),  $9\pi/2 = 14.1372$ , is increased by ten percent, and changed to 15.625. The constant  $9\pi/2$  is determined by the geometry of the sphere. The modification can therefore be interpreted as a change that takes into account, (i) the effects of a soft surface instead of a sharp border, and (ii) the effect of spin-orbit scattering, that changes the lengths of the orbits in a semiclassical description [42]. The modification of this constant is equivalent to define an effective neutron number (cf Eq. (57)),  $N_{eff} \approx 0.91N$ , and that is the way it was included in the calculations.

We can now compare the fluctuating part of the energy obtained for a sphere with the experimental data. The two quantities plotted are  $\tilde{\mathcal{B}}$  for the experimental data (as defined by Eqs.(1) and (51)), and  $\tilde{\mathcal{B}}_{sph}$  for the theory. The result is shown in Fig. 7. It is clear that the simple model of a spherical cavity (with only one adjusted parameter ( $\bar{k}_F R$ ) that has been slightly increased) gives a pretty good semi-quantitative description of all the main features of the shell effects observed in the nuclear masses:

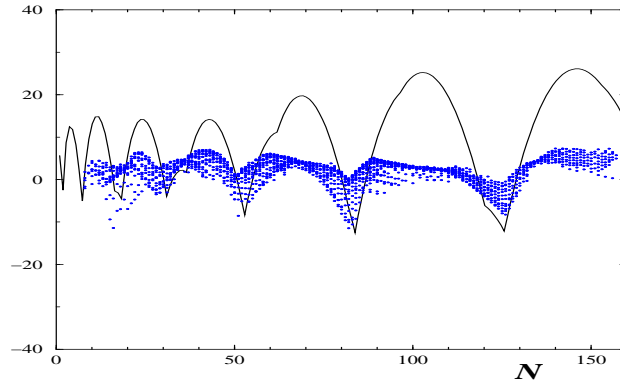


**Fig. 7.** The fluctuating part of the mass of the 1888 nuclei of the 1995 Audi–Wapstra compilation (dots) (cf Fig. 6), compared to the fluctuating part of the energy of a Fermi gas on a spherical cavity (full line).

- 1) the period of the oscillations, that increases with  $N$ , is very well described by the model. The agreement between theory and experiment is particularly good for  $N \geq 25$ , but clear correlations are also observed at lower values of  $N$ .
- 2) the spherical cavity correctly reproduces the asymmetry between sharp minima and rounded maxima.
- 3) the magic numbers obtained from the spherical model, at  $N_{sph} = 2, 7, 18, 30, 52, 83, 126$ , are in good agreement with the experimental values  $N_{exp} = 2, 8, 20, 28, 50, 82, 126$ . As was shown in §4, short orbits dominate the fluctuations of the energy of the gas. In order to get an analytic estimate of the magic numbers, we can simply consider the minima of  $\tilde{B}$  when only the triangular and square orbits are taken into account in Eq. (55). This gives the approximation,

$$N_{magic} \approx \left[ \frac{(2k+1)\pi}{10.77} \right]^3 \approx 9, 18, 33, 55, 84, 122 \dots \quad (59)$$

$k$  is an arbitrary integer number, that has been taken equal to 3, 4, ..., 8 to obtain the values on the r.h.s. The constant 10.77 is computed from the parameters that define both orbits.

- 4) the amplitude of the oscillations is qualitatively correct. However, in Fig. 7 only the neutron contribution is plotted. Clearly, the spherical cavity overestimates the amplitude.
- 5) The overestimate of the amplitude is larger for the maxima. This difference is due to the well-known fact that the nucleus is deformed between closed shells. This is treated in more detail below.

Figure 7 shows a direct comparison of the experimental data to the binding energy of a Fermi gas on a spherical cavity as a function of the neutron

number. At each value of  $N$ , several experimental points appear in the plot, that correspond to different atomic elements that vary by their atomic number  $Z$ . In its present version, the model is too simple to distinguish between different nuclei at a given  $N$ . The more sensible way to proceed is to simply compare  $\tilde{\mathcal{B}}$  to the average of the experimental masses computed at a fixed  $N$ . This average curve is shown, with respect to the original experimental data, in part (a) of Fig. 8. In part (b) the average curve obtained is compared to  $\tilde{\mathcal{B}}$  for a spherical cavity. This figure is thus equivalent to Fig. 7, but with average experimental results.

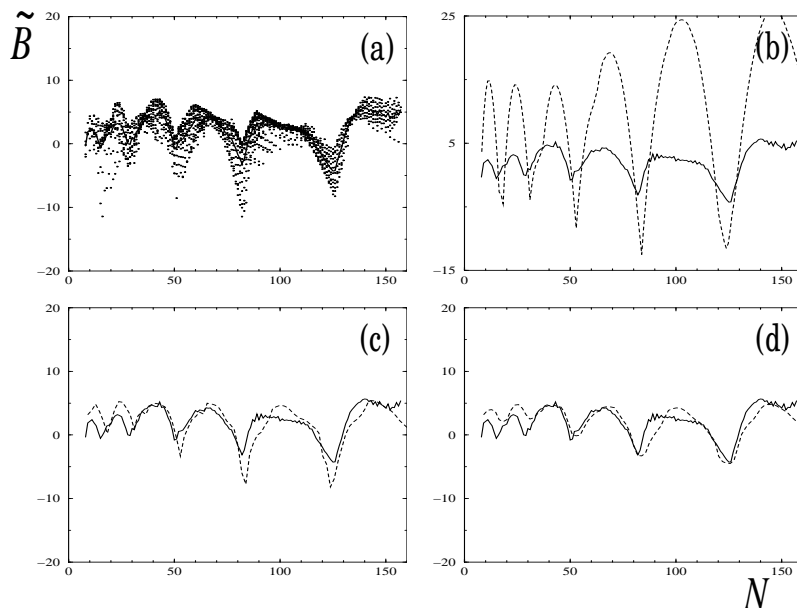


**Fig. 8.** Comparison between different theoretical approximations and experimental values of the fluctuating part of the nuclear masses. (a) Experimental data (dots), with their average behavior (full line). Average experimental data (full line) compared to the predictions of (dashed line) (b) a spherical cavity, (c) a (possibly) deformed cavity, and (d) a (possibly) deformed cavity with a finite coherence length.

The negative peaks of  $\tilde{\mathcal{B}}$  define regions of more stable nuclei. In between magic numbers, the spherical cavity leads to neutron numbers with a positive contribution  $\tilde{\mathcal{B}}$ . These large and positive contributions diminish the binding energy. A possible mechanism to avoid that effect and to increase the stability with respect to the spherical shape in between closed shells is **deformation**. By changing its shape, the nucleus can increase its stability by finding regions where  $\tilde{\mathcal{B}}$  is more favorable. To complete the previous model, it is therefore nec-

essary to incorporate symmetry breaking degrees of freedom. In the new space of deformations, the mass is determined by minimizing, at a fixed particle number, the binding energy with respect to the deformation parameters.

The deformation is here treated as a small perturbation of the spherical shape [43]. An important technical advantage of the perturbative approach is that it leads to a very simple semiclassical treatment, where the deformation is incorporated as a modulation factor into the previous formulas:  $A_{p,r}$  is replaced by  $A_{p,r} \times M_{p,r}(x)$  in Eq. (55) [43].  $x$  denotes the deformation parameters, taken as quadrupole ( $x_2$ ), octupole ( $x_3$ ), and hexadecapole ( $x_4$ ) axial symmetric deformations of the surface of the sphere parametrized, in spherical polar coordinates  $(r, \theta, \phi)$ , by  $r(\theta) = R \left[ 1 + x_0 + \sum_{j=2}^4 x_j P_j(\cos \theta) \right]$ .  $x_0$  is included to ensure volume conservation, and the  $P_j(y)$  are the Legendre polynomials of order  $j$ . The explicit expressions of the modulation factors  $M_{p,r}(x)$  for the three deformations of the periodic orbit families of a spherical cavity may be found in Ref. [41]. Including these factors in the semiclassical expressions, at a fixed neutron number  $N$ , the minimum of the binding energy is located in the parameter space  $(x_2, x_3, x_4)$ .

The results of the minimization procedure for nuclei with neutron number up to 160 are shown in part (c) of Fig. 8. With respect to a perfectly spherical shape, the results are greatly improved and the agreement with the experimental data is much better. The amplitude of the shell corrections have been strongly diminished. The shape and position of the negative peaks of  $\tilde{B}$  remain largely unchanged. The main difference is that the large positive peaks have been suppressed, and replaced by a less pronounced oscillatory behavior.

As a final improvement of the model we consider **inelastic processes**. The model presented above is based on a mean field approach, where each nucleon (or quasiparticle) freely moves in the self-consistent mean field produced by the other nucleons. This single-particle picture is of course an idealized approximation of the full many body problem. In reality, quasiparticles have a finite lifetime associated to inelastic processes. By producing single-particle energy levels with a certain width, nucleon-nucleon inelastic scattering tends to wash out the coherent phenomena that lies behind the shell effects, and manifests as a phase-breaking mechanism. As a consequence, a finite phase coherence length enters now the play, that corresponds to the typical distance a quasiparticle travels without losing phase coherence.

When the finite width of the single-particle levels is included into the semiclassical treatment, the net output is very natural. It manifests as a damping factor in the sum over periodic orbits, that suppresses the contribution of long periodic orbits [30]. This is similar to what happens to shell effects as the temperature of the system is raised [6]. In the approximation (55), the fluctuating part of the energy, including deformations as well as inelastic processes, is obtained by replacing  $A_{p,r}$  by  $A_{p,r} \times M_{p,r}(x) \times \kappa_\xi(\ell_{vw})$ , where  $\kappa_\xi(\ell) = (\ell/\xi) / \sinh(\ell/\xi)$ , and  $\xi$  is the phase coherent length expressed

in units of the radius of the sphere. For orbits whose length  $\ell_{vw} \gg \xi$ , the latter factor produces an exponential damping of the corresponding contribution. In the opposite limit, when  $\ell_{vw} \ll \xi$ ,  $\kappa_\xi$  tends to one. The phase coherence length  $\xi$  measures the typical number of times a quasiparticle can bounce back and forth in the mean field potential before losing phase coherence.

Fixing this length to  $\xi \sim 5$ , the fluctuating part of the binding energy  $\tilde{\mathcal{B}}$  is represented in part (d) of Fig. 8. With respect to part (c), which does not include decoherence phenomena, the amplitude and peaks are diminished, and now the theoretical description provides a very convenient description of the average experimental data. The agreement is less good at small neutron numbers  $N \lesssim 30$ , a foreseeable discrepancy from a theory based on a large  $N$  expansion. The RMS error between the theoretical curve of Fig. 8(d) and the average experimental data is of 1.3 MeV (taking into account only points with  $N \gtrsim 30$ ). This error is only a factor two larger than the best current results of global mass adjustments, a remarkable result considering the simplicity of the model.

Before closing this section on the ability of a spheroidal cavity to reproduce the experimental data, we would like to consider, within the present model, **supershell structures**. These are long-range coherent modulations of the amplitude of the shell oscillations. They constitute a further remarkable manifestation of the collective deviations of the single-particle spectrum with respect to its average behavior. Initially predicted for a spherical cavity by Balian and Bloch [30, 44], they were observed experimentally in metallic clusters [45]. In nuclear physics, in principle the range of variability of the number of nucleons is too small in order to clearly display the effect. However, we will see that, contrary to this expectation, there exist some indications of this effect in the nuclear masses.

The simplest and more elegant formulation of supershells is based on semiclassical arguments. They are associated to the beating pattern produced by the interference of two periodic orbits of the spherical cavity that have similar lengths, the triangle (3,1) and the square (4,1) [30, 44]. When only their contributions are taken into account in Eq. (55), the oscillatory part of the binding energy is approximated by

$$\tilde{\mathcal{B}} \approx CN^{1/6} \cos\left(\frac{\varphi_\Delta - \varphi_\circ}{2}\right) \cos\left(\frac{\varphi_\Delta + \varphi_\circ}{2} + \frac{\pi}{2}\right), \quad (60)$$

where  $C$  is some amplitude factor that has no relevance in the present discussion,  $\varphi_\Delta = 3\sqrt{3} \times 1.98N^{1/3} + 9\pi/4$  and  $\varphi_\circ = 4\sqrt{2} \times 1.98N^{1/3} + 11\pi/4$  are the phases  $\bar{k}_F R \ell_{vw} + \nu_{vw}\pi/2$  associated to the triangle and the square orbits, respectively. This simple equation describes the supershell effect. On the one hand it includes the shells, given by the fast oscillations produced by the second cosine in Eq. (60) (sum of the phases). The approximate magic numbers Eq. (59) were computed by locating the minima of this term. The amplitude of the fast oscillations is modulated, on long range scales, by the

term containing the difference of the phases. These modulations produce a beating pattern of the shell amplitudes. The nodes of this pattern determine the particle numbers where the shells have a minimum amplitude. From Eq. (60), the nodes are located at

$$N_{nodes} \approx \left[ \frac{(2n + 1/2)\pi}{(4\sqrt{2} - 3\sqrt{3}) 1.984} \right]^3 \approx 5, 634, 3699, \dots \quad (61)$$

where  $n = 0, 1, 2, \dots$  is an arbitrary integer number. Atomic nuclei of 630 neutrons are thus necessary to observe one supershell oscillation. In spite of this difficulty, we can however explore if there are traces of the modulation in the available experimental data, having in mind that a node is predicted for  $N \approx 5$ . For that purpose, we plot in Fig. 9 the average experimental curve (defined in part (a) of Fig. 8), and compare it to the modulation factor of the shell oscillations (supershell envelope, dashed line).

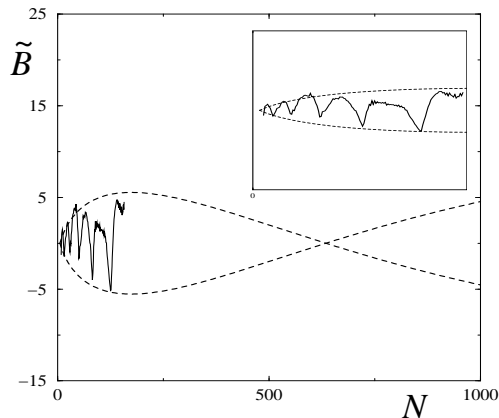


**Fig. 9.** The average fluctuating part of the mass of the 1888 nuclei of the 1995 Audi–Wapstra compilation (full line) compared to the modulation factor of the shell oscillations (supershell envelope, dashed line). The inset shows a closer view of the same curves, where the node at  $N \approx 5$  is visible.

Although the experimental data is indeed not unambiguous due to the limited range of the number of neutrons, it is clear that they follow, to a good approximation, the supershell modulations. It should be noted that the increase of the amplitude observed when going from  $N \sim 10$  to  $N \sim 160$  (better displayed in the inset) cannot be explained by the overall factor  $N^{1/6}$  in Eq. (60). It requires, as a main ingredient, the supershell modulation factor.

The perturbative treatment of a spherical cavity, with an underlying classical regular motion of the nucleons, allows therefore to understand in very simple physical terms most features of the shell fluctuations observed in the



atomic masses. Beyond this specific model, it is possible to use the general arguments introduced in the previous section to estimate the typical size of the shell effects in the nuclear masses to be expected from a generic integrable motion. In the experimental curve, Fig. 6, the fluctuations have approximately constant amplitude, with an RMS size  $\sigma_{exp} \approx 3$  MeV.

A theoretical prediction of the typical size of the fluctuations can be made from the results of §4 (cf Eq. (49) and Ref. [7]). The variance of the binding energy or mass fluctuations of a Fermi gas whose corresponding classical dynamics is regular is given by,

$$\langle \tilde{\mathcal{B}}_{reg}^2 \rangle = \frac{1}{24\pi^4} g E_c^2 . \quad (62)$$

We thus simply need to compute  $g$  and  $E_c$  for the nucleus. The length of the shortest periodic orbit can be estimated as twice the diameter of the nucleus. Its period is  $\tau_{\min} = 4R/v_F$ , where  $R$  is the nuclear radius and  $v_F$  the Fermi velocity. Then, according to the definition (11),

$$E_c = \frac{h}{\tau_{\min}} = \frac{h v_F}{4R} = \frac{\pi \bar{E}_F}{k_F R} .$$

From Eq. (57) (or its generalization to an arbitrary shape), with  $N = A/2$ , we have  $k_F R \approx 1.5A^{1/3}$ . Therefore, using moreover Eq. (58), we obtain,

$$E_c = \frac{80}{A^{1/3}} \text{ MeV} . \quad (63)$$

On the other hand, from Eqs. (15) and (18), putting  $\bar{\mathcal{N}} = A$ , it follows that

$$\delta = \frac{2}{3} \frac{\bar{E}_F}{A} ,$$

and hence,

$$g = \frac{E_c}{\delta} \approx 3 \times A^{2/3} . \quad (64)$$

In Eq. (62), the  $A$  dependence between  $E_c^2$  and  $g$  cancels exactly, and the RMS of the mass fluctuations of a regular motion is, finally,

$$\sigma_{reg} = \sqrt{\langle \tilde{\mathcal{B}}_{reg}^2 \rangle} \approx 2.9 \text{ MeV} , \quad (65)$$

which is in good agreement with the experimental result. For a generic regular dynamics, the size of the mass fluctuations is therefore expected to be constant, e.g. with no dependence on the number of particles. In this respect, the spherical cavity is special. In fact, Eq. (25) shows that the amplitude of all the periodic orbits (except the  $v = 2w$  family, which is of lower weight) scales as  $\epsilon_F^{1/4} \sim A^{1/6}$  (cf Eq. (57)). Therefore, the size of the fluctuations for a spherical cavity scales as  $\sigma_{sph} \sim A^{1/6}$ . In atomic nuclei, this prediction is not

generically valid, due to deformations. But this scaling is expected to hold for the strength of the peaks associated to the magic numbers, where the nucleus is well described by a spherical shape. From a dynamical point of view, the specificity of the sphere compared to a generic regular motion comes from the fact that the codimension of the  $v > 2w$  families of periodic orbits of the sphere is three, whereas the generic codimension for 3D integrable systems is two.

## 5.2 Chaotic motion

The description of the mass fluctuations in terms of a regular nucleonic motion is globally quite satisfactory. However, the semiclassical methods employed here only provide a semi-quantitative description. Actual calculations of the masses are in fact much more sophisticated. Different methods, more or less phenomenological, have been used to produce global systematics of the nuclear masses. These are based on shell model approaches, mean field theories (with or without correlations, using different effective forces), or phenomenological liquid drop models plus shell corrections. The number of adjustable parameters in these theories is considerable, of the order of 20-30. See Ref. [46] for a recent review that describes the different approaches. In spite of the sometimes very different conceptual basis of these models, there is a peculiar common feature that emerges. Over the whole mass chart of known nuclides, the different models possess a comparable precision, of the order of 400 – 700 keV. A typical RMS error with respect to the experimental data, taken from Ref. [47], is shown in Fig. 10 (dots). An error of the order of 500 keV, which decreases with  $A$ , is observed.

Is there a way to understand this deviation? The fact that different models have approximately the same precision points to the fact that there may be a fundamental physical mechanism at work here. In the present framework based on a semiclassical description of the motion of the nucleons, a natural scheme to explore is the presence of some chaotic motion. Although we have argued that a regular motion of the nucleons is energetically more favorable than a chaotic one, there are several reasons that make the presence of the latter inevitable. The first one is that a perfectly regular motion is rather unusual in nature (it holds for the two-body problem with central forces, but the three body is already not integrable). A mixed dynamics, where regular and chaotic motion coexist, is generically expected to occur. There is no simple reason to believe that the full many-body nuclear problem, with of the order of 100 interacting particles, will not follow the generic rule. The second argument in favor of the presence of chaos is also fundamental. As we will argue below, there are indications that what is really computed by assuming some chaoticity in the nucleon's motion are correlation effects that are beyond the mean-field description of the nucleus.

We therefore assume that the phase-space of the nucleons at Fermi energy is dominated by regular components but contains, nevertheless, some

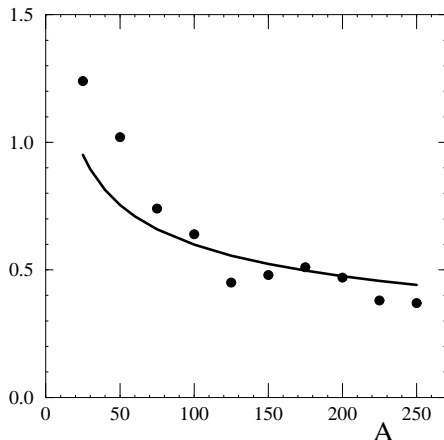


**Fig. 10.** The RMS of the difference between computed and observed masses as a function of the mass number (dots, from Ref. [47]), compared to the RMS of the mass fluctuations due to a chaotic motion. Taken from Ref. [7].

chaotic layers. The idea is to compute the contribution to the mass of these chaotic layers, and then compare it to the deviation observed between the experimental data and the best theoretical predictions. From a semiclassical point of view, the most simple approximation that can be made in the generic case of a mixed dynamics is to split the sum over periodic orbits in Eq. (44) into two terms, one from the regular part, the other from the chaotic phase space sector. The mass fluctuations are now written as,

$$\tilde{\mathcal{B}} = \tilde{\mathcal{B}}_{reg} + \tilde{\mathcal{B}}_{ch} . \quad (66)$$

The two terms on the r.h.s. are, from a statistical point of view, independent,  $\langle \tilde{\mathcal{B}}_{reg} \tilde{\mathcal{B}}_{ch} \rangle = 0$ . This happens because, as already pointed out in §4, the dominant contribution to the energy comes from the short orbits, with  $\tau_p \ll \tau_H$ . Since the orbits contributing to each term are different because they lie in different phase-space regions, the cross product of two different orbits vanishes by the averaging procedure (assuming that the actions of the orbits are incommensurable).

We now need to evaluate the variance of the shell corrections that originate in the chaotic layers of a nucleus, given by the term  $\tilde{\mathcal{B}}_{ch}$  in Eq. (66). We want to make a statistical estimate which, as discussed before, has the advantage of requiring a minimum amount of information about the system. This can be done from the general result obtain in §4, Eq. (49) with  $\beta = 1$  (assuming time reversal symmetry),

$$\langle \tilde{\mathcal{B}}_{ch}^2 \rangle = \frac{1}{8\pi^4} E_c^2 . \quad (67)$$

An estimate of  $E_c$  is now required. In fact, the result obtained previously, Eq. (63), can be used here. The reason is that  $E_c$  is defined as the energy conjugate to the shortest periodic orbit. In a system where regular motion coexists with chaos, the shortest orbit lying in the regular or in the chaotic components will have approximately the same period (or length) at fixed energy  $\overline{E}_F(A, x)$ . Therefore, the scale  $E_c$  associated to each of the contributions in Eq. (66) will be similar.

No other information is needed to estimate the size of the contributions to the mass that originate from the chaotic layers. Using Eq. (63), we obtain,

$$\sigma_{ch} = \sqrt{\langle \tilde{\mathcal{B}}_{ch}^2 \rangle} \approx \frac{2.8}{A^{1/3}} \text{ MeV} . \quad (68)$$

This result has to be compared with the RMS of the difference between the experimental and the computed masses, which we take, as mentioned before, from Ref. [47]. The comparison is shown in Fig. 10.

The agreement is quite good. The amplitude in Eq. (68) is uncertain up to an overall factor of say, 2. It can be varied by increasing slightly the period of the shortest orbit (we have chosen twice the diameter of the nucleus, which is the shortest possible length; any modification, assuming for example a triangular-like shape, or any other shape, will increase the length and period, and therefore will diminish  $\sigma_{ch}$ ), and by a more appropriate inclusion of spin and isospin (this increases  $\sigma_{ch}$  by a factor 2 if these components are treated as uncorrelated). The  $A$  dependence of the error is very well fitted in the region  $A \gtrsim 75$ , with deviations observed at lower mass numbers. This is consistent with the expected loss of accuracy of the semiclassical theories for light nuclei.

There are several features of the present theory – that interprets the mass deviations in terms of chaotic motion – that make its predictions reliable. First of all, Eq. (67) contains only *one physical parameter*, the period of the shortest chaotic periodic orbit, which is a function of  $A$  because the size of the nucleus increases with the mass number. It has no dependence on the relative size of the chaotic region, i.e., on the fraction of phase space occupied by chaotic motion. Without this quite remarkable and important fact we would have been forced to estimate that fraction, something that is hardly possible with present knowledge, despite the efforts in this direction since the pioneering work of Ref. [48]. Mathematically, this is due to the fact that, in chaotic systems, the dominant part of the form factor in the integral (47) is independent of the Heisenberg time (cf Eq. (8)). But it is precisely that time that has information on the corresponding level density  $\delta = \overline{\rho}^{-1}$  (the total average level density of a mixed system is the sum of the average level densities of the regular and chaotic components. Each of these densities is proportional to the phase space volume occupied by the corresponding motion). Therefore, for the chaotic component the integral (47) has no information on the relative phase space volume occupied by the chaotic layers. This information enters only as a correction, through the parameter  $g$  in Eq. (49).

Equation (67) is in fact quite robust. It is not only independent of the chaotic phase-space volume, but it is also valid for arbitrary dimensions. After a system-dependent transient (schematically represented in Fig. 5), the linear growth of the form factor in Eq. (47) for chaotic systems with  $\beta = 1$  is a quite general feature, independent of *any* information of the system. This fact suggests a very natural origin of these fluctuations. Although our analysis is based on a single-particle picture, it can be extended to the full many-body phase space (of dimension  $6 \times A$ ). In that space, and in a semiclassical picture, to first approximation the point representing the system follows a very simple trajectory, driven by the regular mean-field that dominates the motion. On top of that, it is likely that the residual interactions, not taken into account in that approximation, induce chaotic motion. The presence of chaotic orbits would then introduce additional long-range modulations. Eq. (67) would then still be valid to evaluate the amplitude of those modulations, with  $\tau_{min}$  the period of the shortest chaotic orbit in the multidimensional space. Rough estimates indicate that  $\tau_{min}$  is comparable to the three-dimensional non-interacting period (this corresponds, for example, to collective and coherent oscillations of the particles). Therefore Eq. (67) presumably gives an estimate of the mass fluctuations arising from neglected many-body effects. This deserves further investigation, though some work in this direction has already been undertaken [49].

## 6 Conclusions

We have presented in these lectures a study of shell effects on nuclear ground states within a unified framework, namely periodic orbit theory. In a mean-field approximation of the nuclear dynamics, the single-particle motion is quantized. The regular or chaotic nature of the classical single-particle motion imprints the single-particle spectrum in two different ways. The first one occurs at the scale of the mean level spacing  $\delta$ , and produces different (but universal) statistical fluctuations. The second acts on a much larger scale  $E_c$ , set by the inverse of the time of flight across the system. A bunching of the single-particle levels produced by the short periodic orbits is observed on this scale, whose intensity depends on the regular or chaotic nature of the motion. These two features of the single-particle spectrum influence the probability distribution of the quantum fluctuations of thermodynamic functions of the Fermi gas in different ways. In the particular case of the mass, the fluctuations are controlled by the short periodic orbits.

Without need of heavy and numerically expensive many-body calculations, the (phenomenological) semiclassical theory, although less precise, provides a good semi-quantitative explanation of most of the features of the experimental data on nuclear masses. A simple model of regular classical motion based on a spherical cavity (including the possibility of deformations and decoherence effects) gives already a good agreement. Within this model,

the average behavior of the experimental data is reproduced, for nuclei with more than 30 neutrons, with a RMS error of 1.3 MeV. This error is only a factor two larger than the best current results of global mass adjustments, a remarkable result considering the simplicity of the model. This stresses that the main physical effect behind shell effects is purely kinematic, with spin-orbit or other interactions having a small overall influence. The latter were phenomenologically taken into account by adjusting the value of  $\bar{k}_F R$ . Within this simplified model, long range modulations of the shell amplitudes (super-shells) were also investigated. Although, due to a limited particle number, this effects cannot unambiguously be displayed, clearly the present experimental data show some indications of supershell structure in the atomic masses.

When the experimental data is compared with the best global theoretical calculations over the whole mass spectrum, deviations of the order of 500 keV, which decrease with  $A$ , are observed. We interpret this deviation as due to the presence of some chaotic components in the phase space dynamics of the nucleons. Our computations require very little information on the system. In spite of that, they are in good agreement with the deviations observed. Our interpretation does not imply the existence of a “chaotic” insurmountable obstacle that, intrinsically, limitates our understanding and predictive power to compute the nuclear masses (see, in this respect, Ref. [50]). It simply says that at these scales (of the order of 500 keV) a new effect appears that needs to be taken into account properly. The picture we are suggesting is coexistence of order and chaos as produced, for instance, by residual interactions. Further evidence should be given to confirm this scenario. In particular, the theory predicts autocorrelations in the total energies [6], as well as the effect of the presence of chaotic layers on the nuclear level density (as a function of the excitation energy).

## References

1. C. F. von Weizsäcker: *Z. Phys.* **96**, 431 (1935)
2. A. Bohr and B. R. Mottelson: *Nuclear Structure*, (Benjamin, Reading, MS 1969) Vol.I
3. V. M. Strutinsky and A. G. Mägnér: *Sov. J. Part. Nucl.* **7**, 138 (1976)
4. Y. Imry: *Introduction to Mesoscopic Physics*, (Oxford University Press, New York 1997)
5. M. Brack: *Rev. Mod. Phys.* **65**, 677 (1993)
6. P. Leboeuf and A. Monastra: *Ann. Phys.* **297**, 127 (2002)
7. O. Bohigas and P. Leboeuf: *Phys. Rev. Lett.* **88**, 092502 (2002); **88**, 129903 (2002)
8. P. Leboeuf, A. G. Monastra and O. Bohigas: *Reg. Chaot. Dyn.* **6**, 205 (2001)
9. P. Leboeuf and A. G. Monastra: *Nucl. Phys. A* **724**, 69 (2003)
10. C. E. Porter (Ed.): *Statistical Theories of Spectra: Fluctuations*, (Academic Press, New York 1965)

11. Proceedings of the Les Houches Summer School, *Chaos and Quantum Physics* (M.-J. Gianonni, A. Voros and J. Zinn-Justin, Eds.), Les Houches Session LII, (North Holland, Amsterdam 1991)
12. Proceedings of the Les Houches Summer School, *Mesoscopic Quantum Physics*, Les Houches, Session LXI (E. Akkermans, G. Montambaux, J.-L. Pichard and J. Zinn-Justin eds.), (Elsevier 1995)
13. T. Guhr, A. Müller-Groeling, and H. A. Weidenmüller: Phys. Rep. **299**, 189 (1999)
14. Special issue: *Random Matrix Theory*, J. Phys. A **36** (2003)
15. E. P. Wigner: Proc. Cambridge Philos. Soc. **47**, 790 (1951). See also Ref.[10]
16. M.L. Mehta: *Random Matrices*, (Academic Press, New York 1991)
17. K. Efetov: Adv. Phys. **32**, 53 (1983); *Supersymmetry in Disordered and Chaos*, (Cambridge University Press, Cambridge 1997)
18. O. Bohigas, M.-J. Giannoni and C. Schmit: Phys. Rev. Lett. **52**, 1 (1984)
19. O. Bohigas: in Ref. [11], p.87.
20. If the system has discrete symmetries (like the parity symmetry in the cardioid billiard), the statistics of energy levels in each symmetry class should be computed separately
21. A. Baecker: <http://www.physik.tu-dresden.de/~baecker/research.html>.
22. E. Brézin and A. Zee Nucl. Phys. B **402**, 613 (1993)
23. A. Soshnikov: Commun. Math. Phys. **207**, 697 (1999)
24. This statement ignores some well known counterexamples, like the harmonic oscillator with commensurate frequencies
25. J. Marklof: Commun. Math. Phys. **177**, 727 (1996)
26. R. D. Williams and S. E. Koonin: Nucl. Phys. A **391**, 72 (1982)
27. P. Leboeuf and M. Saraceno: Phys. Rev. A **41**, 4614 (1990)
28. M. Brack and R. K. Bhaduri: *Semiclassical Physics*, (Addison-Wesley, Reading, Massachusetts 1997)
29. H. P. Baltes and E. R. Hilf: *Spectra of Finite Systems*, (Bibliographisches Institut-Wissenschaftsverlag, Mannheim 1976)
30. R. Balian and C. Bloch: Ann. Phys. (N.Y.) **69**, 76 (1972)
31. M. C. Gutzwiller: J. Math. Phys. **12**, 343 (1971); *Chaos in Classical and Quantum Mechanics*, (Springer, New York 1990)
32. M. V. Berry: Proc. Roy. Soc. Lond. A **400**, 229 (1985)
33. J. Hannay and A. M. Ozorio de Almeida: J. Phys. A **17**, 3429 (1984)
34. M. Sieber and K. Richter: Phys. Scr. T **90**, 128 (2001)
35. L. Landau and E. M. Lifchitz: *Physique Statistique*, (Éditions Mir, Moscou 1988)
36. V. M. Strutinsky: Nucl. Phys. A **122**, 1 (1968); see also H. A. Bethe: Ann. Rev. Nucl. Sci. **21**, 93 (1971)
37. V. M. Strutinsky: Nucl. Phys. A **95**, 420 (1967)
38. M. Brack, J. Damgaard, A. S. Jensen, H. C. Pauli, V. M. Strutinsky, and C. Y. Wong: Rev. Mod. Phys. **44**, 320 (1972)
39. G. Audi and A. H. Wapstra: Nucl. Phys. A **595**, 409 (1995)
40. B. Povh, K. Rith, C. Scholz, and F. Zetsche: *Particles and Nuclei: an introduction to the physical concepts*, (Springer-Verlag, New York 1995)
41. P. Meier, M. Brack, and S. C. Creagh: Z. Phys. D **41**, 281 (1997)
42. R. G. Littlejohn and W. G. Flynn: Phys. Rev. A **45**, 7697 (1992); H. Frisk and T. Guhr: Ann. Phys. **221**, 229 (1993)

43. S. C. Creagh, *Ann. Phys. (N.Y.)* **248**, 60 (1996)
44. H. Nishioka, K. Hansen, and B. R. Mottelson, *Phys. Rev. C* **42**, 9377 (1990).
45. W. D. Knight, W. A. de Heer, W. A. Saunders, M. Y. Chou, and M. L. Cohen, *Phys. Rev. Lett.* **52**, 2141 (1984)
46. D. Lunney, J. M. Pearson, and C. Thibault: *Rev. Mod. Phys.* **75**, 1021 (2003)
47. P. Möller, J. R. Nix, W. D. Myers, and W. J. Swiatecki: *At. Data and Nucl. Data Tables* **59**, 185 (1995)
48. R. Arvieu, F. Brut, J. Carbonell, and J. Touchard: *Phys. Rev. A* **35**, 2389 (1987)
49. J. G. Hirsch, A. Frank, V. Velazquez: nucl-th/0306049; J. G. Hirsch, V. Velazquez, A. Frank: nucl-th/0308038
50. S. Aberg: *Nature* **417**, 499 (2002)